

AD-A062 332

SCIENCE APPLICATIONS INC MCLEAN VA

F/G 7/4

SOFT X-RAY PHOTOEMISSION AND CHARGE DEPOSITION NEAR MATERIAL IN--ETC(U)

AUG 78 D J STRICKLAND, D L LIN, V W PINE

F19628-77-C-0181

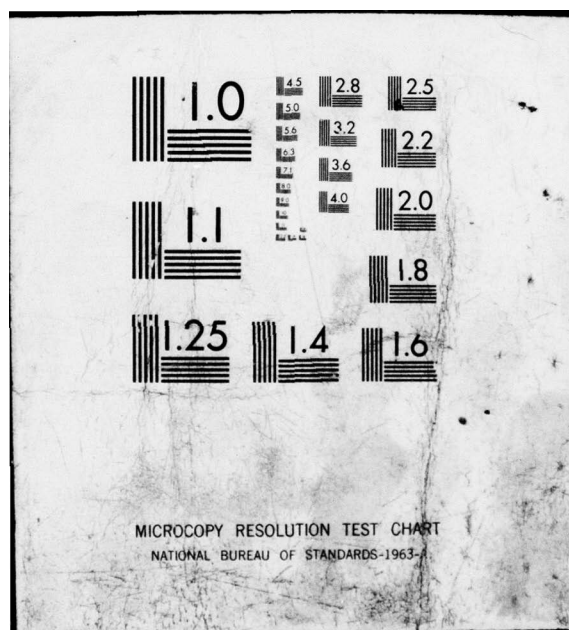
UNCLASSIFIED

RADC-TR-78-183

NL

1 OF 2
AD
A062332





LEVEL

AD A062332

RADC-TR-78-183
Final Technical Report
August 1978

SOFT X-RAY PHOTOEMISSION AND CHARGE DEPOSITION NEAR MATERIAL
INTERFACES

D. J. Strickland
D. L. Lin
V. W. Pine
W. L. Chadsey

Science Applications Inc.

DDC FILE COPY

Approved for public release; distribution unlimited.

This research was sponsored by the Defense Nuclear Agency
under Subtask Z99QAXTA040, Work Unit Code 71 entitled
"Electron Transport Phenomenology."

ROME AIR DEVELOPMENT CENTER
Air Force Systems Command
Griffiss Air Force Base, New York 13441

78 12 13

This report has been reviewed by the RADC Information Office () and is releasable to the National Technical Information Service (NTIS). At NTIS it will be releasable to the general public, including foreign nations.

RADC-TR-78-183 has been reviewed and is approved for publication.

APPROVED:

John C. Garth

JOHN C. GARTH
Contract Monitor

APPROVED:

Robert M. Barrett

ROBERT M. BARRETT
Director
Solid State Sciences Division

FOR THE COMMANDER:

John P. Huss

JOHN P. HUSS
Acting Chief, Plans C

If your address has changed or if you wish to be removed from the mailing list, or if the addressee is no longer employed by your organization, please notify RADC (ESR), Hanscom AFB MA 01730.

Do not return this copy. Retain or destroy.

UNCLASSIFIED

SECURITY CLASSIFICATION OF THIS PAGE (When Data Entered)

REPORT DOCUMENTATION PAGE		READ INSTRUCTIONS BEFORE COMPLETING FORM
1. REPORT NUMBER RADC-TR-78-183	2. GOVT ACCESSION NO.	3. RECIPIENT'S CATALOG NUMBER N/A
4. TITLE (and Subtitle) SOFT X-RAY PHOTOEMISSION AND CHARGE DEPOSITION NEAR MATERIAL INTERFACES	5. TYPE OF REPORT & PERIOD COVERED Final Technical Report 17 Oct 77 - 1 Feb 78	6. PERFORMING ORG. REPORT NUMBER N/A
7. AUTHOR(s) D. J. Strickland, W. L. Chadsey D. L. Lin V. W. Pine	8. CONTRACT OR GRANT NUMBER(s) F19628-77-C-0181	
9. PERFORMING ORGANIZATION NAME AND ADDRESS Science Applications Inc 1651 Old Meadow Road Suite 600 McLean VA 22101	10. PROGRAM ELEMENT, PROJECT, TASK AREA & WORK UNIT NUMBERS 62704H CDNA0027	
11. CONTROLLING OFFICE NAME AND ADDRESS Deputy for Electronic Technology (RADC/ESR) Hanscom AFB MA 01730 Monitor/John C. Garth/ESR	12. REPORT DATE August 1978	13. NUMBER OF PAGES 100
14. MONITORING AGENCY NAME & ADDRESS (if different from Controlling Office) Same	15. SECURITY CLASS. (of this report) UNCLASSIFIED	15a. DECLASSIFICATION/DOWNGRADING SCHEDULE N/A
16. DISTRIBUTION STATEMENT (of this Report) Approved for public release; distribution unlimited.		
17. DISTRIBUTION STATEMENT (of the abstract entered in Block 20, if different from Report) Same CDNA, Z99QAXT		
18. SUPPLEMENTARY NOTES This research was sponsored by the Defense Nuclear Agency under Subtask Z99QAXTA040, Work Unit Code 71 entitled, "Secondary Electron Transport Phenomenology." RADC Project Engineer: John Garth (ESR)		
19. KEY WORDS (Continue on reverse side if necessary and identify by block number) Soft X-Ray Photoemission Electron Backscatter Charge Deposition		
20. ABSTRACT (Continue on reverse side if necessary and identify by block number) The work reported here comes under two distinct headings: (1) soft x-ray photoemission and (2) charge deposition profiles near irradiated material interfaces. The first electron backscatter results using the SXRP code are reported. Good agreement is obtained with measurements for 5 keV electrons incident on Al. The effect of elastic scattering on the photoemission spectrum is analyzed in further detail following the initial observations made in a previous DNA contract. Additional code validation tests plus the good agreement with measurements for backscatter confirm the (CONT'D)		

DD FORM 1 JAN 73 1473

EDITION OF 1 NOV 65 IS OBSOLETE

UNCLASSIFIED

SECURITY CLASSIFICATION OF THIS PAGE (When Data Entered)

408 404
18 12 13 008

UNCLASSIFIED

SECURITY CLASSIFICATION OF THIS PAGE(When Data Entered)

20 (CONT'D)

previous result that scattering significantly effects the photoemission spectrum. A simple technique is presented which relates the inner shell ionization IMFP to the corresponding photoionization cross section. The technique is tested on the K and L shells of Al and gives IMFP's which agree well with more rigorous results. The development of an empirical photoemission code is reported along with spectra and yields for exploding wire sources incident on Al, Au, Ag, and C. Finally charge deposition profiles for several material configurations containing thin foils are obtained with the POEM code and compared with data by Frederickson. In general, good agreement is achieved.

UNCLASSIFIED

SECURITY CLASSIFICATION OF THIS PAGE(When Data Entered)

TABLE OF CONTENTS

	<u>Page</u>
Section 1: INTRODUCTION AND SUMMARY.....	8
Section 2: FURTHER INVESTIGATION INTO THE EFFECT OF SCATTERING ON THE PHOTOEMISSION SPECTRUM.....	15
Section 3: ELECTRON BACKSCATTER FROM Al FOR 5 keV INCIDENT ELECTRONS.....	21
Section 4: A SIMPLE TECHNIQUE FOR OBTAINING INNER SHELL IMFP's FROM PHOTOABSORPTION COEFFICIENTS.....	27
Section 5: A CODE FOR EMPIRICALLY PREDICTING PHOTOEMISSION AND ITS APPLICATION TO PHOTOEMISSION FROM Al, Au, Ag, AND C FOR AN EXPLODING WIRE RADIATION SOURCE... 30	30
Section 6: CHARGE DEPOSITION PROFILE NEAR ⁶⁰ Co IRRADIATED MATERIAL INTERFACES.....	48
REFERENCES.....	53

ADDITIONAL	
RTIS	White Section <input type="checkbox"/>
DOC	Buff Section <input checked="" type="checkbox"/>
UNANNOUNCED	<input type="checkbox"/>
JUSTIFICATION.....	
BY.....	
DISTRIBUTION/AVAILABILITY CODES	
Dist.	AVAIL. and/or SPECIAL
A	

LIST OF TABLES

	<u>Page</u>
TABLE 1. BACKSCATTER YIELDS Y_{BS} FOR THE INCIDENT FLUX GIVEN BY EQUATIONS (6)-(8) AND THEIR CORRESPONDING YIELDS rY_{BS} ADJUSTED TO NORMAL INCIDENCE. THE CONSTANT C IS THE FACTOR SCALING $K_{elas}(E)$. THE MEASURED VALUE FOR COMPARISON WITH rY_{BS} IS $\sim .17$	26
TABLE 2. ATOMIC SHELLS TREATED IN THIS WORK AND THEIR BINDING ENERGIES IN keV.....	36
TABLE 3. AUGER MODEL FOR Au, Ag, Al, AND C.....	38
TABLE 4. TRANSITION PROBABILITY RELATED INFORMATION FOR THE M SHELL OF GOLD (ω , a, and S are defined in the text.).....	40
TABLE 5. BURKE'S EMPIRICAL PARAMETER β VERSUS Z.....	42
TABLE 6. TOTAL YIELDS IN ELECTRONS/PHOTON FOR THE SOURCE SPECTRA IN FIGURES 1-3.....	45
TABLE 7. CONFIGURATIONS FOR CALCULATIONS.....	49
TABLE 8. COMPONENTS OF CURRENT.....	51

LIST OF FIGURES

	<u>Page</u>
FIGURE 1. Photoemission Spectra for an 8 keV Photon Source Incident on Al.....	56
FIGURE 2. Source Distribution of Photo- and Auger Electrons for the 8 keV Gaussian Photon Source Used to Perform the SXRP Calculations.....	57
FIGURE 3. SXRP Photoelectron Spectra at Various Depths for 8 keV Photons Incident on Al. Each Spectrum Gives the Electrons Passing Through a Unit Area in the Back Direction.....	58
FIGURE 4. Energy Dependence of Screening Parameters and Corresponding Elastic IMFP's Used to Perform the Backscatter Calculations for Al.....	59
FIGURE 5. Assumed Angular Dependence of the Incident Electrons and the Backscatter Yield.....	60
FIGURE 6. Differential and Cumulative Backscatter Yields for the Various Representations of the Elastic Scattering Cross Sections Described in the Text.....	61
FIGURE 7. A Comparison on Inner Shell IMFP's Given by Integrating Equation (10) and by Ashley, et al. ¹¹ From More Rigorous Calculations....	62
FIGURE 8. The Photoabsorption Coefficients Used to Calculate the IMFP's Shown in Figure 7.....	63
FIGURE 9. Photoabsorption Cross Sections for Al.....	64
FIGURE 10. Photoabsorption Cross Sections for Au.....	65
FIGURE 11. Photoabsorption Cross Sections for Ag.....	66
FIGURE 12. Photoabsorption Cross Sections for C.....	67

LIST OF FIGURES (Continued)

	<u>Page</u>
FIGURE 13. Range and Stopping Power for Al.....	68
FIGURE 14. Range and Stopping Power for Au.....	69
FIGURE 15. Range and Stopping Power for Ag.....	70
FIGURE 16. Range and Stopping Power for C.....	71
FIGURE 17. The First of Four Photon Spectra Used to Study the Sensitivity of Photoemission to Variations in the EWR Source.....	72
FIGURE 18. The Second of Four Photon Spectra Considered.....	73
FIGURE 19. The Remaining Two Photon Spectra for Performing the Sensitivity Analysis.....	74
FIGURE 20. Differential Yields for Al Obtained with the Transport Code for Photon Spectra ②-④	75
FIGURE 21. Empirical Differential Yields for Al for Photon Spectra ①-④	76
FIGURE 22. Empirical Total Yields versus Photon Energy for Au.....	77
FIGURE 23. Empirical Differential Yields for Au for Photon Spectra ①-④	78
FIGURE 24. Empirical Differential Yield Components for Au for Photon Spectrum ②	79
FIGURE 25. Empirical Differential Yields for Ag for Photon Spectra ①-④	80
FIGURE 26. Empirical Differential Yields for C for Photon Spectra ① ④	81
FIGURE 27. Transport Geometry.....	82

LIST OF FIGURES (Concluded)

	<u>Page</u>
FIGURE 28. Currents in the foils for the Al/Al/Pb Configuration.....	83
FIGURE 29. Charge Deposition Profile for the Al/Al/Pb Configuration.....	84
FIGURE 30. Charge Deposition Profile for the Pb/Al/Al Configuration.....	85
FIGURE 31. Charge Deposition Profile for the Pb/Sn/Sn Configuration.....	86
FIGURE 32. Charge Deposition Profile for the Sn/Sn/Al Configuration.....	87
FIGURE 33. Charge Deposition Profile for the Al/Ta/Al Configuration.....	88

Section 1

INTRODUCTION AND SUMMARY

The work performed for this contract comes under three distinct headings. They are

- (1) User's Guide to X-Ray Dose Enhancement,
- (2) Soft X-Ray Photoemission, and
- (3) Charge Deposition Profiles Near Irradiated Material Interfaces.

W. L. Chadsey and V. W. Pine participated in the work under headings (1) and (3) while D. J. Strickland and D. L. Lin carried out the work on soft x-ray photoemission. The User's Guide has been separately prepared by W. L. Chadsey. Thus, topics (2) and (3) will be discussed in this report.

The work carried out on soft x-ray photoemission is a continuation of work supported over the past two years by DNA and AFSC.¹⁻³ During that time,

¹ D. J. Strickland, "Soft X-Ray Photoemission," RADC-TR-77-252, (July 1977).

² D. J. Strickland, D. L. Lin, T. M. Delmer, S. Rodgers, B. Goplen, and W. L. Chadsey, "Soft X-Ray Photoemission, II," DNA Final Report, Submitted October 1977.

³ W. L. Chadsey, B. L. Beers, V. W. Pine, D. J. Strickland, and C. W. Wilson, "X-Ray Photoemission; X-Ray Dose Enhancement," RADC-TR-77-253, (July, 1977).

the soft x-ray photoemission code SXRP was developed and applied to aluminum (Al), aluminum oxide (Al_2O_3), and silicon dioxide (SiO_2) for narrow Gaussian photon sources used to simulate line sources, for blackbody spectra, and for an exploding wire radiator (EWR) spectrum. For line sources, good agreement in total yield was obtained between SXRP calculations and measurements for photoemission from Al over the photon energy range from ~ 1 to 10 keV. Furthermore, excellent agreement was achieved with Bradford's total yield for a 50 kVp bremsstrahlung source.

A detailed sensitivity analysis was then carried out for Al to determine the sensitivity of both the total and differential photoemission yields to inverse mean free paths (IMFP's) for elastic and inelastic electron interactions, to the initial photoelectron angular distribution, and to variations in photon spectra. An important result of this analysis was that scattering produces a significant effect on the shape of the photoemission spectrum as well as on the total yield. The work discussed in Sections 2 and 3 of this report was prompted by this observation.

Other noteworthy work pertained to a comparison between SXRP calculations and measurements of the photoemission spectrum and total yield for an EWR source incident on Al . The comparison led to a significant readjustment of one set of data obtained with a magnetic spectrometer and to the conclusion that the data from a second experiment involving biased diodes could not be used to obtain a satisfactory emission spectrum. Details appear in the final report

just completed for DNA.² This study has ultimately led to a better basic understanding of photoemission for an EWR source and defined the limits of the experiments.

Under this contract, there were several objectives in the continued study of soft x-ray photoemission. They may be generally classified as follows:

- (1) to perform backscatter calculations using the SXR code,
- (2) to further analyze the effect of scattering on the photoemission spectrum,
- (3) to begin specifying the needed atomic information for new materials [specifically for gold (Au), silver (Ag), and carbon (C)], and
- (4) to provide, in a brief period of time an approximate representation of photoemission from Au, Ag, and C for an EWR source.

The backscatter calculations were performed both to increase the applicability of the SXR code and to

² D. J. Strickland, D. L. Lin, T. M. Delmer, S. Rodgers, B. Goplen, and W. L. Chadsey, "Soft X-Ray Photoemission, II," DNA Final Report, submitted October, 1977.

critically test the elastic scattering cross section representation in the code. The immediate need for this test was to determine if the strength of the scattering effect observed on the photoemission spectrum was real or due in part to an inaccurate representation of the elastic scattering cross section.

Objectives (3) and (4) relate to DNA's SKYNET program, part of which involves the specification of photoemission from various materials irradiated by an EWR source. As a start in examining these materials, the needed atomic information was assembled for performing empirical photoemission calculations based on the Burke model.⁴ The empirical approach was initiated to quickly obtain spectral and total yield information for the immediate purpose of supporting SGEMP code validation experiments. Work is now underway which will extend this effort by providing SXRPs results for the additional materials.

The results of the work of soft x-ray photoemission are as follows:

- (1) Good agreement in backscatter between SXRPs results and measurements was obtained for 5 keV electrons incident on Al.
- (2) The SXRPs code successfully meets the following conditions as applied to photoelectron transport.

⁴ E. A. Burke, "Soft X-Ray Induced Electron Emission," IEEE Trans. Nuc. Sci., NS-24, No. 6, 2505, (1977).

- the bulk solution is independent of scattering,
 - the photoelectron spectrum does not change with depth in the absence of scattering.
- (3) The above results plus those from previous tests provide convincing evidence that the SXR code is accurately predicting the effect of scattering on the photoemission spectrum. The effect, which is to reduce the surface spectrum compared to the bulk spectrum in those spectral regions dominated by electrons having lost appreciable energy, is strong even under the simplifying conditions of a uniform isotropic photoelectron source.
- (4) The photoemission spectrum measured by Denisov et. al.⁵ for 8 keV photons incident on Al closely resembles the bulk spectrum and is thus not a satisfactory representation of the photoemission spectrum.
- (5) A technique has been developed which relates the IMFP's for inner shell

⁵ E. P. Denisov, V. N. Shchmelev, A. N. Mezhevich, and M. A. Rumsh, "Analysis of the Energy Structure of X-Ray Photoemission from a Massive Cathode," *Fix. Tver. Tela*, 6, 2569 (1964) [*Sov. Phys.-Solid State* 6, 2047 (1965)].

ionization to the corresponding photoionization cross sections. The method has been applied to Al and gives K- and L- shell IMFP's which agree well with independent results. The technique provides an important new capability which will be used to specify currently unavailable inner shell IMFP's for new materials.

- (6) Empirically derived photoemission spectra and total yields have been obtained for Al, Au, Ag, and C for four representations of an EWR source. In general, the yield is not particularly sensitive to the choice of photon spectra considered but is to the material. Gold, e.g., photoemits about 20 times stronger than carbon for an EWR source.

For the third task in this contract, the POEM code was used to calculate charge deposition profiles for several material configurations irradiated by a ^{60}Co x-ray source. The calculated profiles were then compared to the measurements by Frederickson.⁶ Each configuration consisted of a series of thin foils sandwiched between two thicker slabs of material, each

⁶ A. R. Frederickson, "Charge Deposition Profiles Near Irradiated Material Interfaces," IEEE Trans. Nuc. Sci., NS-23, No. 6, 1867, (1976).

greater than an electron range thick for the most energetic photoelectrons. The materials considered were Al, Sn, Ta, and Pb. Results will be presented in Section 6 for six different configurations. To summarize, good agreement was obtained between the calculations and measurements near material interfaces having large atomic number differences. Best agreement was achieved for an Al-Al-Pb configuration with the least satisfactory agreement for an Sn-Sn-Al configuration.

Section 2

FURTHER INVESTIGATION INTO THE EFFECT OF SCATTERING ON THE PHOTOEMISSION SPECTRUM

One of the most important results obtained to date in our soft x-ray photoemission program is that scattering has a pronounced effect on the shape of the photoemission spectrum and its total yield even under the simplifying assumptions that the photoelectron source is uniform and isotropic. Our initial observations were made using an 8 keV photon source incident on Al. This source was chosen since, to our knowledge, it is the only one for which spectral data on photoemission from Al exists over an extended energy range.⁵ We found that a serious discrepancy existed between our results and the data. A further problem was the excellent agreement Burke achieved with the data using his empirical model.⁴ This model is based on the assumptions that the photoelectron source is uniform and isotropic, and that the electrons lose energy continuously. To account for scattering, Burke introduced a material dependent reflection

⁴ E. A. Burke, "Soft X-Ray Induced Electron Emission," IEEE Trans. Nuc. Sci., NS-24, No. 6, 2505 (1977).

⁵ E. P. Denisov, V. N. Shchemelev, A. N. Mezhevich, and M. A. Rumsh, "Analysis of the Energy Structure of X-Ray Photoemission from a Massive Cathode," Fiz. Tver. Tela, 6, 2569 (1964) [Sov. Phys.-Solid State 6, 2047 (1965)].

parameter which typically reduces his total yield by ~50%. The effect of scattering was not, however, taken into account in obtaining the shape of the photoemission spectrum.

Based upon these considerations, a series of SXRP runs was made with a uniform, isotropic photoelectron source and with varying degrees of scattering to see if Burke's spectral shape could be achieved in the limit of zero scattering. The code was, in fact, able to closely reproduce Burke's result which provided an important test on the treatment given to scattering.

Figure 1 summarizes the state of affairs prior to the work performed under this contract. Most of these results have already appeared (in log-log form) in a recent DNA final report.² The features peaking at 7.5, 6.2, and 1.4 keV are due to L-photo, K-photo, and KLL Auger electrons respectively. The angular integrated source spectrum used in the calculations is shown in Figure 2. The K- and L- photoelectron features are Gaussian distributions like the 8 keV photon source while the KLL Auger feature is triangular in shape with a width of only 0.2 keV.

To further investigate the observed effect of scattering on the photoemission spectrum, we have

² D. J. Strickland, D. L. Lin, T. M. Delmer, S. Rodgers, B. Goplan, and W. L. Chadsey, "Soft X-Ray Photoemission, II," DNA Final Report, submitted October, 1977.

examined the behavior of our photoelectron solutions as a function of depth under various scattering conditions and (2) have performed backscatter calculations using the SXR code. Step (1) provides additional means of validating the code while step (2) provides a sensitive test of the applied elastic scattering IMFP.

We can conclude from the backscatter results plus new photoemission results to be presented in the next figure, that the difference between the SXR spectrum and measurement shown in Figure 1 is not due to a faulty representation of the elastic scattering IMFP. The calculated spectrum obtained prior to this work, is not, however, based on the best value of the scattering parameter η_c (defined in Section 3). A value $\eta_c = 3.2$ should have been used instead of $\eta_c = 1.0$ based on the work of Nigam, et al.⁷ which came to our attention while investigating the elastic scattering IMFP in considerably more detail than in earlier work. The backscatter calculations discussed in Section 3 confirm the observation that the larger η_c is more appropriate. We have rerun the SXR code for $\eta_c = 3.2$ and find that the photoemission spectrum does not significantly change. Spectra will be shown shortly for $\eta_c = 3.2$, $\eta_c = 1.0$ as well as for Moliere's η_c which will demonstrate this fact. We include results for Moliere's η_c since this representation has commonly been used in the past in multiple scattering transport

⁷ B. P. Nigam, M. K. Sundaresan, and Ta-You Wu, "Theory of Multiple Scattering: Second Born Approximation and Corrections to Moliere's Work," Phys. Rev. 115, 491 (1959).

calculations. It is not the best representation in our formulation, however, based on considerations of low energy electrons interacting with the screened Coulomb field of an atom in a solid. Further details on this subject will be reported under the current DNA contract on soft x-ray photoemission.

The purpose for examining the depth dependence of our photoelectron solutions rests on the following known facts:

- (1) In the absence of scattering, the surface solution (photoemission spectrum) must equal the bulk solution and
- (2) In the bulk region, the solution cannot be a function of scattering.

We find that the SXRP code satisfies both of these conditions. In the absence of scattering the calculated photoelectron spectrum is constant with depth to within a few percent. With a full scattering treatment, the calculated spectrum comes to within a few percent of the non-scattering result at depths well away from the surface. This is shown in Figure 3 where the photoelectron spectrum is given at depths of 0, 10^{-5} , and 10^{-4} cm for the three choices of η_c discussed above. We see for a given representation of η_c , that the spectrum at 10^{-4} cm is essentially the same as the non-scattering surface spectrum in Figure 1.

We do note some differences in the surface spectrum from one η_c to the next although the scattering effect being addressed in this section is of about the same magnitude for all cases. The best surface spectrum is given for $\eta_c = 3.2$.

To explain the effect shown in Figure 3 (for a given η_c), we simply note that, in the bulk, the spectrum contains more electrons which have lost appreciable energy. For example, the bulk spectrum contains ~ 4 times more electrons than the surface spectrum at 2 keV, an energy at which the electrons have lost a minimum of 4 keV. In the bulk, many of these electrons originate in the fore hemisphere somewhat closer to the surface and then scatter into the back hemisphere. To make the transition requires a large number of scatterings and is accompanied by significant energy loss. As one approaches the surface, there are fewer electrons available in the fore hemisphere for contributing to the flux in the back hemisphere due to the decrease in available volume. This results in a decrease in the spectrum in its large energy loss regions.

In conclusion, we have offered additional evidence that the SXR code is correctly predicting the extent to which scattering affects the photoemission spectrum. It has been shown that the code

- (1) obtains photoelectron spectra independent of depth in the absence of scattering,

- (2) obtains the same bulk solution with or without scattering, and
- (3) gives good backscatter results for 5 keV electrons incident on Al (next section).

In addition, it has been previously shown that the code

- (4) gives good agreement with photoemission yield data for line sources incident on Al over the photon energy range from ~ 1 to 10 keV, and
- (5) reproduces the shape and magnitude of the empirical photoemission spectrum in the absence of scattering (the total yield for either approach is about twice too large with no scattering corrections).

Based on the evidence presented, neither the data by Denisov, nor the bulk photoelectron spectrum, nor the empirical photoemission spectrum, all of which are very similar, give an accurate representation to the photoemission spectrum. The true spectrum shows greater variations with energy due to the effect of scattering as represented by the SXRP calculations.

Section 3

ELECTRON BACKSCATTER FROM Al FOR 5 keV INCIDENT ELECTRONS

The purpose of the backscatter calculations reported in this section was to test the accuracy of our representation of the elastic scattering IMFP for Al in the low kilovolt region. Our immediate interest was to know if elastic scattering is being adequately described in SXR calculations for an 8 keV photon source discussed in Section 2.

We use the screened Rutherford formula to specify the elastic scattering IMFP. It's differential form is given by

$$K_{\text{elas}}(E, \theta) = K_{\text{elas}}(E) p(E, \theta) \text{ cm}^{-1} \text{sr}^{-1} \quad (1)$$

where

$$p(E, \theta) = \frac{\eta(\eta+1)}{\pi} \frac{1}{(1-\cos+2\eta)^2} \quad (2)$$

$p(E, \theta)$ is the normalized Rutherford formula and η is the screening parameter which contains the energy dependence in p . $K_{\text{elas}}(E)$ has the form

$$K_{\text{elas}}(E) = n \frac{Z^2 e^4}{v^2 p^2} \frac{\pi}{\eta(\eta+1)} \quad (3)$$

where v and p are respectively the electron velocity and momentum corresponding to E , Z is the atomic number, and η is the material number density. The screening parameter η may be represented in the form

$$\eta(E) = 4.3 Z^{2/3} \frac{\eta_c}{E} \quad (4)$$

where E is in eV and η_c is a function of the screening potential. The screening potential in conducting solids can be adequately represented by a single Yukawa potential which leads to constant η_c .⁷ We will consider the values $\eta_c = 1$ and 3.2. We have previously used $\eta_c = 1$ since values close to unity have been applied before.^{8,9} The value 3.2 appears more appropriate since it is based on considerations of the screening potential itself.⁷

Moliere has presented an energy dependent form for η_c which has had wide application to multiple scattering calculations at high energy. It is given by

$$\eta_c = 1.13 + 3.76 \left(\frac{Z}{137v/c} \right)^2 \quad (5)$$

⁷ B. P. Nigam, M. K. Sundaresan, and Ta-You Wu, "Theory of Multiple Scattering: Second Born Approximation and Corrections to Moliere's Work," Phys. Rev. 115, 491 (1959).

⁸ M. J. Berger, S. M. Seltzer, and K. Maeda, "Energy Deposition by Aurola Electrons in the Atmosphere," J. Atmos. Terr. Phys., 32, 1015 (1970).

⁹ H. E. Bishop, "Electron Scattering in Thick Targets," Brit. J. Appl. Phys., 18, 703, (1967).

Results will also be presented for this η_c primarily to show the sensitivity of backscatter to different representations of $K_{elas}(E, \theta)$. We do not suggest the use of Moliere's η_c at low energies in our formulation which is based on a single scattering description, i.e. where each type of electron event is modelled in detail.

For the three η_c 's just discussed, Figure 4 shows the resulting screening parameters and the elastic IMFP's. The energy range extends down to the lower limit treated in the present calculations.

The point of the present backscatter calculations, as stated above, was to test the values of $K_{elas}(E)$ and $p(E, \theta)$ which have been used in photo-emission calculations. In particular, we are interested in initial electron energies in the vicinity of 5 keV which dominate the electron source spectrum for the 8 keV photon source we have been using to investigate the effect of scattering on the photo-emission spectrum. The incident electron flux we have chosen is Gaussian in both E and μ and peaks at 5 keV. Designating the incident flux by $\phi_0(E, \mu)$ ($\phi_0 = \phi(z=0, E, \mu > 0)$) it is given by

$$\phi_0(E, \mu) = f(E)g(\mu) \quad \text{el/cm}^2\text{-sec-eV-sr} \quad (6)$$

with

$$f(E) = \frac{4}{\sqrt{\pi}} \exp \left[- \left(\frac{E-5}{.25} \right)^2 \right] \quad (7)$$

and

$$g(\mu) = \frac{10}{\sqrt{\pi}} \exp \left[- \left(\frac{1-\mu}{.2} \right)^2 \right] \quad (8)$$

The functions f and g are both normalized over their respective ranges. The choice of width for $f(E)$ is not critical since the backscatter coefficient or yield for Al varies slowly with energy at 5 keV. The choice of width for $g(\mu)$ was dictated by the number of μ points used in the calculations (20). $g(\mu)$ does not give an effective representation of normal incidence but this is not necessary for the testing of $K_{\text{elas}}(E)$ and $p(E, \theta)$ since we are able to adjust our backscatter yields for comparison with available data which are typically taken at normal incidence. The adjustment factor is simply

$$r = \frac{Y(\mu=1)}{\int_0^1 g(\mu) Y(\mu) d\mu} \quad (9)$$

where $Y(\mu)$ is the backscatter yield as a function of μ , the cosine of the incidence angle. $Y(\mu)/Y(1)$ is shown in Figure 5 along with $g(\mu)$. The shape of $Y(\mu)$ was taken from Bishop for 10 keV electrons incident on Al.⁹ We expect the shape of $Y(\mu)$ at 5 keV to be similar based on, e.g., the work of Bishop⁹ and

⁹ H. E. Bishop, "Electron Scattering in Thick Targets," Brit. J. Appl. Phys., 18, 703, (1967).

Darlington and Cosslett.¹⁰ The resulting value of r is .75 which will be applied shortly.

For the incident flux given by equations (6)-(8), Figure 6 shows the differential and cumulative backscatter yields for four different representations of $K_{elas}(E, \theta)$. Table 1 gives the total yields as well as adjusted values for normal incidence based on $r = .75$. Three of the cases considered refer to equations (1)-(3) with $\eta_c = 1$, $\eta_c = 3.2$, and Moliere's η_c . The fourth is given by Moliere's η_c with $K_{elas}(E)$ scaled down by a factor of 2. This case is included just to show the sensitivity of backscatter to the magnitude of $K_{elas}(E)$ holding the mean angle of scattering fixed or equivalently holding η fixed. For what we believe to be the best representation of K_{elas} , i.e., for $\eta_c = 3.2$, the backscatter yield is 21% which when corrected for non-normal incidence is 16%. This is in excellent agreement with measurements of this quantity.⁴ The Moliere representation also gives excellent agreement with the data as well as with the differential yield above 2 keV for $\eta_c = 3.2$. The agreement between the two representations is due to the intersection of their η 's near 4 keV which is in the region primarily responsible for the backscatter characteristics. We see that the yield is quite sensitive to the scaling of $K_{elas}(E)$. There is nearly a one-to-one correspondence between the yield and scaling factor for the given material and given energy. There is much less sensitivity, however, if instead of charging the

⁴ E. A. Burke, "Soft X-Ray Induced Electron Emission," IEEE Trans. Nuc. Sci., NS-24, No. 6, 2505, (1977).

¹⁰ E. H. Darlington and V. E. Cosslett, "Backscattering of 0.5 - 10 keV Electrons from Solid Targets," J. Phys. D: Appl. Phys., 5, 156, (1972).

overall magnitude of K_{elas} by scaling, the magnitude is changed using a different dependence in η . For example, $K_{elas}(E)$ for $\eta_c = 1$ is significantly different than for Moliere's η_c (Figure 4) although the corresponding backscatter yields are similar. This results from nearly compensating effects due to the mean angle of scattering changing with η .

TABLE 1. BACKSCATTER YIELDS Y_{BS} FOR THE INCIDENT FLUX GIVEN BY EQUATIONS (6)-(8) AND THEIR CORRESPONDING YIELDS rY_{BS} ADJUSTED TO NORMAL INCIDENCE. THE CONSTANT C IS THE FACTOR SCALING $K_{elas}(E)$. THE MEASURED VALUE FOR COMPARISON WITH rY_{BS} is $\sim .17$.

η_c	C	Y_{BS} (el/el)	rY_{BS} (el/el)
3.2	1	0.21	0.16
1	1	0.29	0.22
Moliere	1	0.21	0.16
"	0.5	0.12	0.09

Section 4

A SIMPLE TECHNIQUE FOR OBTAINING INNER SHELL IMFP'S FROM PHOTOABSORPTION COEFFICIENTS

The SXR code requires IMFP's for the various types of electron interactions in solids. An important interaction, especially for high Z materials, is inner shell ionization. There is currently little information available on IMFP's for this process. The choice of materials previously investigated using the SXR code (Al , Al_2O_3 , and SiO_2) was dictated by the availability of such information.^{11,12} There is now interest in extending the applicability of the SXR code to new materials, in particular to Au, Ag, and C for which the needed IMFP information is not available. This has led us to develop the technique reported herein. Following a brief discussion of the method, IMFP's will be presented for Al and compared with independent results.

We designate the inner shell DIMFP by $K_i(E', W)(\text{cm}^{-1}\text{-ev}^{-1})$ for the i^{th} shell where E' is the incident electron energy and W is the energy loss.

- ¹¹ J. C. Ashley, C. J. Tung, V. E. Anderson and R. H. Ritchie, "Inverse Mean Free Path, Stopping Power, CSDA Range, and straggling in Aluminum and Aluminum Oxide for Electrons of Energy ≤ 10 keV," Report No. AFCRL-TR-75-0583 (December 1975).
- ¹² C. J. Tung, J. C. Ashley, V. E. Anderson, and R. H. Ritchie, "Inverse Mean Free Path, Stopping Power, CSDA Range, and Straggling in Silicon and Silicon Dioxide for Electrons of Energy ≤ 10 keV," Report No. RADC-TR-76-125 (1976).

W may be given by either $E' - E$ or by $E_s + B_i$ where E is the outgoing energy of the degraded incident electron, E_s is the energy of the secondary electron, and B_i is the binding energy for the i^{th} shell. The relationship we have derived between K_i and $\mu_i(h\nu)$, the photoabsorption coefficient is the following:

$$K_i(E', W) = C \frac{\mu_i(h\nu)}{E'h\nu} \ln \frac{(h\nu)^2 + 4E'(h\nu - B_i)}{(h\nu)^2} \quad (10)$$

where the energy loss W is equated to $h\nu$ and the constant C is

$$C = \frac{R_y}{\pi\alpha} \quad (11)$$

R_y is the Rydberg energy (12.6 eV) and α is the fine structure constant (1/137). The energies E' and $h\nu$ are in the units of electron volts.

Expression (10) is based upon

- (1) the Born approximation,
- (2) using the dipole term in the expansion of the generalized oscillator strength, and
- (3) allowing the momentum of the incident electron to be shared by the two outgoing electrons.

To obtain the IMFP $K_i(E')$, equation (10) is integrated over $h\nu$ from B_i to E' . Most of the contribution to $K_i(E')$ comes from $h\nu$ values near B_i since $h\nu$ is smallest and μ_i is largest there. Figure 7 shows $K_i(E')$ for the K and L shells of Al as well as more exact calculations by Ashley, et al.¹¹ The absorption coefficients μ_K and μ_L used in equation (10) are shown in Figure 8. At energies above the peak in either IMFP (K or L), excellent agreement is achieved with the more exact values. The overshoot below the peaks can be attributed to the Born approximation which always leads to an overestimate of K_i near threshold. We are now in the process of incorporating a correction factor to improve the results in this region.

The agreement shown in Figure 7 is significant to our overall program in soft x-ray photoemission since it suggests that equation (10) can provide reasonable values of the inner shell IMFP for new materials. The needed quantities, $\mu_i(h\nu)$ and B_i are readily available for most materials. In actual practice, however, the total absorption coefficient $\mu(h\nu)$ is usually the available experimental quantity which must be decomposed into its separate parts. One can, however, do this with sufficient accuracy to provide a good approximate representation of the needed IMFP's.

¹¹ J. C. Ashley, C. J. Tung, V. E. Anderson, and R. H. Ritchie, "Inverse Mean Free Path, Stopping Power, CSDA Range, and Straggling in Aluminum and Aluminum Oxide for Electrons of Energy ≤ 10 keV," Report No. AFCRL-TR-75-0583 (December 1975).

Section 5

A CODE FOR EMPIRICALLY PREDICTING PHOTOEMISSION AND ITS APPLICATION TO PHOTOEMISSION FROM Al, Au, Ag, AND C FOR AN EXPLODING WIRE RADIATION SOURCE

In this section, we discuss a code developed under this contract which is based on Burke's empirical model for photoemission.⁴ The code calculates the total and differential photoemission yields for an arbitrary photon spectrum. This can be a set of lines, a continuum, or a combination of both.

The primary motivation for generating the code came from SAI's involvement in SGEMP code validation experiments sponsored by DNA. We were seeking an approximate representation of the photoemission spectrum for an EWR source incident on Au, Ag and C. An additional reason for generating the code was to provide information against which SXRP results could be compared. This is particularly useful when there are no other data available for comparison.

The needed relationships for line and continuum sources are presented next. This is

⁴ E. A. Burke, "Soft X-Ray Induces Electron Emission," IEEE Trans. Nuc. Sci., NS-24, No. 6, 2505 (1977).

followed by a presentation of the required input data for the materials Al, Au, Ag, and C. Empirical photoemission results are then given for four representations of an EWR source which show both the general features of photoemission for the various materials and the sensitivity of the yield and spectral shape to changes in the photon source spectrum.

The basic empirical expressions for the transport of electrons produced by monoenergetic photon sources were originally presented by Schaefer.¹³ They are based on the assumptions of:

- depth independent isotropic electron production,
- continuous energy loss, and
- straight line paths of electrons from creation to escape.

The effect of scattering was accounted for by assuming the penetration range was half the total range. Burke has recently modified Schaefer's expressions by using a reflection coefficient to account for scattering rather than halving the range. The expressions below will contain Burke's coefficient. We begin by giving the yield expressions for line source [Equations (12)-(15)]. The corresponding expressions for a

¹³ R. R. Schaefer, J. Appl. Phys. 44, 152 (1973).

continuum source will follow [Equations (17)-(20)].
The total yield for a given photoelectron component is:

$$Y_i(h\nu) = \frac{(1-\beta)}{4} \mu_i(h\nu) R(h\nu - B_i) \text{ electrons/photon} \quad (12)$$

where μ_i is the photoabsorption coefficient (cm^{-1}) for producing the i^{th} type of photoelectron and R is the continuous slowing down approximation (CSDA) range (cm). Its argument contains the starting kinetic energy of the photoelectron where B_i is the i^{th} binding energy. The parameter β is Burke's reflection coefficient. The assumed values of β will be presented later.

The corresponding expression for the j^{th} Auger electron for the i^{th} type of vacancy is:

$$Y_{ij}^A(h\nu) = \frac{(1-\beta)}{4} w_{ij} \mu_i(h\nu) R(E_{ij}^A) \text{ electrons/photon} \quad (13)$$

where w_{ij} is the ij^{th} Auger yield and E_{ij}^A is the starting energy of the ij^{th} Auger electron.

The corresponding differential yields for photo- and Auger electrons are:

$$\frac{dY_i(h\nu, E)}{dE} = \frac{(1-\beta)}{4} \frac{1}{S(E)} \mu_i(h\nu) \quad (14)$$

electrons/photon-keV

$$(E \leq h\nu - B_i)$$

and

$$\frac{dY_{ij}^A(h\nu, E)}{dE} = \frac{(1-\beta)}{4} \frac{w_{ij}}{S(E)} \mu_i(h\nu) \quad (15)$$

electrons/photon-keV

$$(E \leq E_{ij}^A)$$

where $S(E)$ is the stopping power (eV/cm).

Integration of the differential yields from the starting energy to zero gives the total yields since the CSDA range is related to the stopping power by

$$R(E_{\max}) = \int_0^{E_{\max}} \frac{dE}{S(E)} \quad (16)$$

For a continuum source, the above yields become

$$Y_i = \frac{(1-\beta)}{4} \frac{1}{F} \int_{B_i}^{h\nu_{\max}} I(h\nu) \mu_i(h\nu) R(h\nu - B_i) dh\nu \quad (17)$$

$$Y_{ij}^A = \frac{(1-\beta)}{4} \frac{w_{ij}}{F} R(E_{ij}^A) \int_{B_i}^{h\nu_{\max}} I(h\nu) \mu_i(h\nu) dh\nu \quad (18)$$

$$\frac{dY_i(E)}{dE} = \frac{(1-\beta)}{4} \frac{1}{FS(E)} \int_{E+B_i}^{h\nu_{\max}} I(h\nu) \mu_i(h\nu) dh\nu \quad (19)$$

$$\frac{dY_{ij}^A(E)}{dE} = \frac{(1-\beta)}{4} \frac{w_{ij}}{FS(E)} \int_{E+B_i}^{h\nu_{\max}} I(h\nu) \mu_i(h\nu) dh\nu \quad (20)$$

where I is the photon spectrum (photons/cm²-sec-eV) and F is the total number of photons/cm²-sec given by

$$F = \int_{h\nu_{\min}}^{h\nu_{\max}} I(h\nu) dh\nu \quad (21)$$

We have programmed all of the above yield expressions into the empirical code. As noted earlier, the code can treat either one or more lines, a pure continuum, or a combination of lines plus continuum. Total and differential yields are printed out for each type of photoelectron and Auger electron considered, along with their sums.

The basic data needed for the empirical calculations are:

- photoabsorption coefficients $\mu_i(h\nu)$,
- CSDA range $R(E)$,
- Stopping power $S(E)$,
- Auger energies E_{ij}^A and yields w_{ij}^A , and
- Reflection coefficient β .

We begin by presenting Table 2 which contains the shells and their binding energies, as modeled in this work for Au, Ag, Al, and C. We do not include the K shell of Ag nor the K or L shells of Au since their binding energies lie above the energy range of interest for EWR sources.

Figures 9-12 show the photoabsorption cross sections (cm^2) for the four materials. In each figure, individual shell contributions are shown along with their sum. The total cross section is based on information from Biggs and Lighthill,¹⁴ Storm and Israel,¹⁵ and Hubbell.¹⁶ The extrapolations of individual cross sections were made by the authors.

¹⁴ F. Biggs and R. Lighthill, Report No. SC-RR-71-0507, Sandia Laboratories, (1971).

¹⁵ E. Storm and H. I. Israel, Report Number LA-3753, Los Alamos Scientific Laboratory, (1967).

¹⁶ J. H. Hubbell, Atomic Data, 3, 241, (1971).

TABLE 2. ATOMIC SHELLS TREATED IN THIS
WORK AND THEIR BINDING ENERGIES IN keV

MATERIAL	SHELLS	BINDING ENERGY
Au	M ₁	3.425
	M ₂	3.150
	M ₃	2.743
	M ₄	2.291
	M ₅	2.206
	N	0.083
	O ₂₃	0.052
	O ₄₅	0.008
Ag	L	3.351
	M	0.367
	N	0.005
Al	K	1.560
	L	0.073
	M	0.005
C	K	0.284
	L	0.013

Stopping powers and ranges for the four materials are given in Figures 13-16. The information comes from Ashley, et. al.¹⁷ (Au and Ag), Ashley, et. al.¹¹ (Al), and the Bethe formula¹⁸ (C).

Our model for the relevant Auger spectroscopy is given in Table 3. The model serves its one basic requirement - the proper accounting of the bulk of potential energy of inner shell vacancies. For most transitions shown in the table, several Auger lines exist although one will usually be dominant.¹⁹ The energy shown is the energy of the dominant line.

We have given special attention to gold since it is an important material in satellite systems and since its Auger spectroscopy is complicated. If one refers to, e.g., the handbook of Auger electron spectroscopy,¹⁹ it will be seen that basically three pairs of lines exist between 1.5 and 2.1 keV along with two strong lines at 0.069 and 0.239 keV. There are no other important Auger features in the soft x-ray

-
- ¹¹ C. J. Tung, J. C. Ashley, V. E. Anderson, and R. H. Ritchie, Report No. RADC-TR-76-125 (1976).
- ¹⁷ J. C. Ashley, C. J. Tung, R. H. Ritchie, and V. E. Anderson, Report No. RADC-TR-76-220, (June 1976).
- ¹⁸ J. D. Jackson, Classical Electrodynamics, Chapter 13 2nd ed., John Wiley and Sons, Inc. New York, N. Y. (1975).
- ¹⁹ Handbook for Auger Electron Spectroscopy, Physics Electronics Industries, Inc., (1976).

TABLE 3. AUGER MODEL FOR Au, Ag, Al, AND C

MATERIAL	TRANSITION	ENERGY (keV)	YIELD
Au	M ₁ NN	2.111	0.35
		2.024	0.52
		1.772	0.13
	M ₂ NN	2.111	0.35
		2.024	0.52
		1.772	0.13
	M ₃ NN	2.111	0.35
		2.024	0.52
		1.772	0.13
	M ₄ NN	2.111	0.35
		2.024	0.52
		1.772	0.13
	M ₅ NN	2.111	0.35
		2.024	0.52
		1.772	0.13
Ag	NNO	0.239	0.11
	NOO	0.069	0.89
Ag	LMM	2.570	0.90
	MNN	0.351	1.00
Al	KLL	1.400	0.96
	LMM	0.070	1.00
C	KLL	0.272	1.00

region. The three pairs of lines arise from MNN transitions, the 0.239 keV line from an NNO transition, and finally the 0.069 keV line from an NOO transition. In our model given in Table 3, the pairs of lines have been combined giving us a total of five features. This is explained below.

The three MNN features arise from vacancies in the M_4 and M_5 subshells. There are no important lines associated with M_{123} NN transitions since vacancies in the M_1 - M_3 subshells have a high probability of moving up to the M_4 and M_5 subshells. This is illustrated in Table 4 taken from McGuire.²⁰ ω_{M_i} is the probability of fluorescence, a_{M_i} is the probability of a radiationless transition M_iXY with $X \neq M$ and $Y \neq M$, and $S_{M_{ij}}$ is the average number (not probability) of M_j vacancies occurring in a direct transition starting with an M_i vacancy. $S_{M_{ij}}$ will be greater than the corresponding probability of producing at least one M_j vacancy from an M_i vacancy when a super Coster-Kronig transition $M_iM_jM_j$ is energetically possible since, in number, this produces two M_j vacancies. Therefore, the sum

$$\omega_{M_i} + a_{M_i} + \sum_{j>i} S_{M_{ij}}$$

can be greater than unity as is the case for $i=3$ in the table.

Since a vacancy initially created in the M_1 , M_2 , and M_3 subshells transfers to the M_4 and M_5

²⁰ E. J. McGuire, Phys. Rev. A5, 1043, (1972).

TABLE 4. TRANSITION PROBABILITY RELATED INFORMATION
FOR THE M SHELL OF GOLD

(ω , a , and S are defined in the text.)

	$\omega_{M_i}^i$	a_{M_i}	$S_{M_i, i+1}$	$S_{M_i, i+2}$	$S_{M_i, i+3}$	$S_{M_i, i+4}$
M_1	0.002	0.074	0.148	0.594	0.067	0.112
M_2	0.004	0.114	0.114	0.673	0.095	—
M_3	0.004	0.158	0.114	0.782	—	—
M_4	0.026	0.928	0.046	—	—	—
M_5	0.026	0.974	—	—	—	—

subshells with nearly unit probability, we can assign the M_{45} NN Auger energies and yields to M_1 , M_2 and M_3 vacancies. We have made this assignment in our model as illustrated in Table 3.

The final piece of input information is β , Burke's reflection coefficient. Values of β for the four materials appear in Table 5. We used Burke's empirical expression for β :

$$\beta = 0.475 Z^{0.177} - 0.40 \quad (22)$$

The basic quantity to be discussed in this section is the differential yield $dY(E)/dE$ in units of electrons/photon-keV. For each of the four materials, we will provide comparisons of dY/dE for the source spectra shown in Figures 17-19. This will provide the first estimate of the sensitivity of photoemission to variations in the EWR source, as well as provide, in our opinion, the best available photoemission spectral information for Au, Ag, Al, and C using this source.

We begin by considering the material Al which has recently been studied in detail by us using our SXR transport code under the DNA Contract DNA-001-77-0209. Since we have transport results available for Al for spectra 2, 3 and 4 given in Figures 18 and 19, we first present these in Figure 20. All photoemission spectra are dominated by KLL Auger electrons whose initial

TABLE 5. BURKE'S EMPIRICAL
PARAMETER β VERSUS Z

Z	MATERIAL	β
6	Carbon	0.25
13	Aluminum	0.35
47	Silver	0.54
79	Gold	0.63

energy is 1.4 keV. The low energy peak is due to LMM Auger electrons and K-photoelectrons. Empirical results for all four source spectra are shown in Figure 21. A significant decrease in the photoemission yield is observed for spectrum 4 because this spectrum contains ~50% of its photons below the Al 1.56 keV K-edge. Such photons produce little photoemission.

By including the transport results shown in Figure 20, we are able to demonstrate the degree of accuracy of the empirical spectra in Figure 21. We note that there is qualitative agreement, but significantly less structure in the empirical results. The greater structure in the transport results is caused by elastic scattering which is not treated by the empirical method. A detailed discussion of this effect has been given in Section 3. The following word of caution should be given - the degree of difference between empirical and transport results can be expected to be material dependent. We thus reserve comment on the accuracy of the empirical photoemission spectra for the other materials which have not yet been modeled for transport calculations.

The next material we consider is gold. Because it is a complicated material to model, our first empirical results were obtained for monoenergetic photon sources for the purpose of comparison with available data. This comparison is given in Figure 22 in terms of total yield in electrons/photon from $h\nu = 10$ keV down to 0.1 keV. The data were taken from Figure 15 of Burke's paper.⁴

⁴ E. A. Burke, "Soft X-Ray Induced Electrom Emission," IEEE Trans. Nuc. Sci., NS-24, No. 6, 2505 (1977).

In general, our empirical results are $\sim 25\%$ below both the data and Burke's results. We have not resolved the discrepancy as of this time. Part of the difference will be due to more detail given to the subshell contributions in our formulation.

The yield dY/dE for the four source spectra for Au obtained by the empirical code appear in Figure 23. In general, the spectra are harder for Au than for Al and show more sensitivity to the source spectra. The softer, less structured yields for photon spectra 3 and 4 result from these spectra having no photons above 2.2 keV and thus not allowing for M shell ionization. To provide insight into the results for Au, dY/dE for source spectrum 2 is shown in Figure 24 in terms of its many components for Auger and photoelectrons. We see that the Au spectrum is harder than the Al spectrum because of the MNN Auger and N shell photoelectron emission.

The empirical results for Ag and C appear in Figures 25 and 26. We observe that the emission spectra are not very sensitive to differences between the first three source spectra, except at high electron energies.

To conclude this section, we give the integrated yields in Table 6 for the four materials and four source spectra. Au and C provide the highest and lowest yields, respectively. The Au yields may be too low based on the 25% difference between the empirical results and the data for line sources shown previously in Figure 22. For Al the empirical yield is $\sim 30\%$ higher than the transport yield. In general, the numbers in this table should be

TABLE 6. TOTAL YIELDS IN ELECTRONS/PHOTON
FOR THE SOURCE SPECTRA IN FIGURES 1-3

Multiply the numbers by 10^{-3} .

	SPECTRUM			
	1	2	3	4
Al-TRANSPORT	—	7.0	7.1	5.6
Al-EMPIRICAL	9.9	10.1	10.1	6.2
Au-EMPIRICAL	13.2	12.5	8.9	11.3
Ag-EMPIRICAL	7.4	7.5	7.6	9.8
C-EMPIRICAL	0.68	0.69	0.71	0.90

accurate to 50% or less based on Burke's success in reproducing total yield data for a wide variety of materials.

One must not draw general conclusions from Table 6 about relative emission efficiencies from one material to the next. One such mistaken conclusion might be that aluminum emits photoelectrons nearly as efficiently as gold. In general, gold is a better photoemitter. Aluminum happens to be a strong photoemitter for EWR sources since a significant fraction of the photons lies just above the Al K-edge. If the EWR spectrum were shifted as little as 0.2 keV toward lower energy, the Al yield would drop more than a factor of two. It should be emphasized that the photoemission efficiency depends critically on the distribution of photons with respect to the photoabsorption edges for a given material.

To summarize this section, an empirical photoemission code has been developed to provide an additional means of making comparisons with SXRPF results and to provide estimates of photoemission yields for materials not yet treated by the SXRPF code. The purpose of this section has been to document the contents of the empirical code and present our first analysis using this code. The needed atomic information has been presented for the four materials considered - Au, Ag, Al, and C. For Au, Ag, and C, the given data represents our first attempt to model these materials and, consequently, may undergo revisions in anticipated future analyses.

Differential yields were presented for four different source spectra to establish the sensitivity of the photoemission spectrum, as well as total yield to variations in the EWR source. Empirical results were presented for all four materials. Transport results were also presented for Al, not only to show sensitivity to the source spectrum, but also to compare with the empirical emission spectra.

Gold was shown to possess the hardest spectrum and highest yield. It also exhibited a greater sensitivity to the various source spectra considered than the other materials. We believe the transport results for Al and empirical results for Au, Ag, and C presented in this report to be the best such information currently available for an EWR source.

Section 6

CHARGE DEPOSITION PROFILES NEAR ^{60}Co IRRADIATED MATERIAL INTERFACES

Recent experimental work by Frederickson⁶ has provided the users of transport codes with a large data base which may be used for code validation of charge deposition profiles near irradiated material interfaces. Results were presented for charge deposition in thin foils (<0.004 electron range) of Al, Sn, or Ta between various combinations of equilibrium thick slabs of Al, Cu, Sn, or Pb. The radiation source was ^{60}Co γ -radiation.

Calculations of a few configurations have been performed using the one-dimensional version of the POEM²⁵ code. A diagram of the transport geometry is shown in Figure 27. For these calculations, the photons were assumed normally incident upon the surface. The energy spectrum used was the test spectrum integrated over angle.⁶ The configurations considered are shown in Table 7.

⁶ A. R. Frederickson, "Charge Deposition Profiles Near Irradiated Material Interfaces," IEEE Trans. Nuc. Sci., NS-23, No. 6, 1867 (1976).

²⁵ W. L. Chadsey, "POEM: A Fast Monte Carlo Code for the Calculation of X-Ray Photoemission and Transition Zone Dose and Current," AFCRL-TR-75-0323 (15 January 1975).

TABLE 7. CONFIGURATIONS FOR CALCULATIONS

SLAB 1	FOIL	SLAB 2
Al	Al	Pb
Pb	Al	Al
Pb	Sn	Sn
Sn	Sn	Al
Al	Ta	Al
Sn	Ta	Pb

The charge deposition calculations for the given configurations provide a very stringent test of the transport code. The charge deposition is given as a difference between two values of the current which are nearly equal as a result of the thinness of the foils. Agreement between the calculations and measurements, thus provides a high degree of confidence in the POEM code.

For each configuration, six components of the current were calculated as illustrated in Table 8 for the Al/Al/Pb configuration. The net current in the foils is given by

$$J_{\text{net}} = J_{\text{eq}} + (J_1 - J_2) + (J_3 - J_4) + (J_5 - J_6) \quad (23)$$

where J_{eq} is the equilibrium current in Al and the subscripts refer to the components defined in Table 8. The charge deposition in each foil was obtained as the difference in current at the left and right faces of the foil. In general, the net current J_{net} is determined by small differences between the dominant components which are of nearly the same magnitude. Furthermore, the charge deposition in a given foil is the difference in net current at the two surfaces of the foil. The difference is small since the foils are thin. Therefore, high accuracy is required in the Monte Carlo calculations of the current. The current contributions 1 through 6 are shown in Figure 28 for the Al/Al/Pb configuration.

In order to accurately calculate the charge deposition, a minimum of 20,000 electron histories were

TABLE 8. COMPONENTS OF CURRENT

COMPONENT	SLAB 1	FOILS	SLAB 2	ELECTRON SOURCE
1	Al	Al	Pb	Emission from Slab 2 (Pb)
2	Al	Al	Al	Emission from Slab 2 (Al)
3	Al	Al	Pb	Backscatter from Slab 2 (Pb) of electrons emitted from foils
4	Al	Al	Al	Backscatter from Slab 2 (Al) of electrons emitted from foils
5	Al	Al	Pb	Emission from Slab 1 (Al)
6	Al	Al	Al	Emission from Slab 1 (Al)

followed for each contribution. Each of these contributions was fitted within a function of the form

$$J = J_0 \exp(Ax+Bx^2+Cx^3) \quad (24)$$

and the coefficients were determined by a least squares fit to the calculated results. The fits were then evaluated to determine the charge deposition.

The results for the first five configurations shown in Table 7 are presented in Figures 29-33 with the same units used in Reference 6. The histograms are the POEM results and the data points with error bars are the Frederickson results. The agreement between the experimental results and the calculations is, in general, quite good; the results of the calculation in most cases fall within the experimental error bars. Where discrepancies occur, they appear to be statistical in nature, such that the inclusion of more histories in the Monte Carlo calculation would reduce the discrepancies. The calculational results for the Sn/Ta/Pb configuration were quite noisy, in some instances having a different sign than the data. The charge deposition is small in this case, but about the same magnitude found for the Pb/Al/Al configuration. The reason for this discrepancy is not known at this time.

REFERENCES

1. D. J. Strickland, "Soft X-Ray Photoemission," RADC-TR-77-252 (July 1977).
2. D. J. Strickland, D. L. Lin, T. M. Delmer, S. Rodgers, B. Goplen, and W. L. Chadsey, "Soft X-Ray Photoemission, II," DNA Final Report, submitted October 1977.
3. W. L. Chadsey, B. L. Beers, V. W. Pine, D. J. Strickland, and C. W. Wilson, "X-Ray Photoemission; X-Ray Dose Enhancement," RADC-TR-77-253 (July 1977).
4. E. A. Burke, "Soft X-Ray Induced Electron Emission," IEEE Trans. Nuc. Sci., NS-24, No. 6, 2505 (1977).
5. E. P. Denisov, V. N. Shchemelev, A. N. Mezhevich, and M. A. Rumsh, "Analysis of the Energy Structure of X-Ray Photoemission from a Massive Cathode," Fiz. Tver. Tela, 6, 2569 (1964) [Sov. Phys.-Solid State 6, 2047 (1965)].
6. A. R. Frederickson, "Charge Deposition Profiles Near Irradiated Material Interfaces," IEEE Trans. Nuc. Sci., NS-23, No. 6, 1867 (1976).
7. B. P. Nigam, M. K. Sundaresan, and Ta-You Wu, "Theory of Multiple Scattering: Second Born Approximation and Corrections to Moliere's Work," Phys. Rev. 115, 491 (1959).
8. M. J. Berger, S. M. Seltzer, and K. Maeda, "Energy Deposition by Auroral Electrons in the Atmosphere," J. Atmos. Terr. Phys., 32, 1015 (1970).
9. H. E. Bishop, "Electron Scattering in Thick Targets," Brit. J. Appl. Phys., 18, 703 (1967).
10. E. H. Darlington and V. E. Cosslett, "Backscattering of 0.5 - 10 keV Electrons from Solid Targets," J. Phys. D. Appl. Phys., 5, 156 (1972).

REFERENCES (Continued)

11. J. C. Ashley, C. J. Tung, V. E. Anderson, and R. H. Ritchie, "Inverse Mean Free Path, Stopping Power, CSDA Range, and Straggling in Aluminum and Aluminum Oxide for Electrons of Energy 10 keV," Report No. AFCRL-TR-75-0583 (December 1975).
12. C. J. Tung, J. C. Ashley, V. E. Anderson, and R. H. Ritchie, "Inverse Mean Free Path, Stopping Power CSDA Range, and Straggling in Silicon and Silicon Dioxide for Electrons of Energy 10 keV," Report No. RADC-TR-76-125 (1976).
13. R. R. Schaefer, J. Appl. Phys., 44, 152 (1973).
14. F. Biggs and R. Lighthill, Report No. SC-RR-71-0507, Sandia Laboratories, (1971).
15. E. Storm and H. I. Israel, Report Number LA-3753, Los Alamos Scientific Laboratory, (1967).
16. J. H. Hubbell, Atomic Data, 3, 241 (1971).
17. J. C. Ashley, C. J. Tung, R. H. Ritchie, and V. E. Anderson, Report Number RADC-TR-76-220, (June 1976).
18. J. D. Jackson, Classical Electrodynamics, Chapter 13, 2nd ed., John Wiley and Sons, Inc., New York, New York, (1975).
19. Handbook of Auger Electron Spectroscopy, Physics Electronics Industries, Inc., (1976).
20. E. J. McGuire, Phys. Rev., A5, 1043, (1972).
21. E. P. Savinov, A. P. Lukirskii, and Yu. F. Shepelev. Sov. Phys. - Solid State 6, 2624, (1965).
22. E. P. Savinov and A. P. Lukirskii, Optics and Spectroscopy, 23, 163 (1967)
23. L. G. Eliseenko, V. N. Shehemelev, and M. A. Rumsh, Sov. Phys. - JETP 25, 211, (1967).

REFERENCES (Concluded)

24. J. L. Gaines and R. A. Hansen, J. Appl. Phys., 47, 3923, (1976).
25. W. L. Chadsey, "POEM: A Fast Monte Carlo Code for the Calculation of X-Ray Photoemission and Transition Zone Dose and Current, AFCRL-TR-75-0324, (15 January 1975).

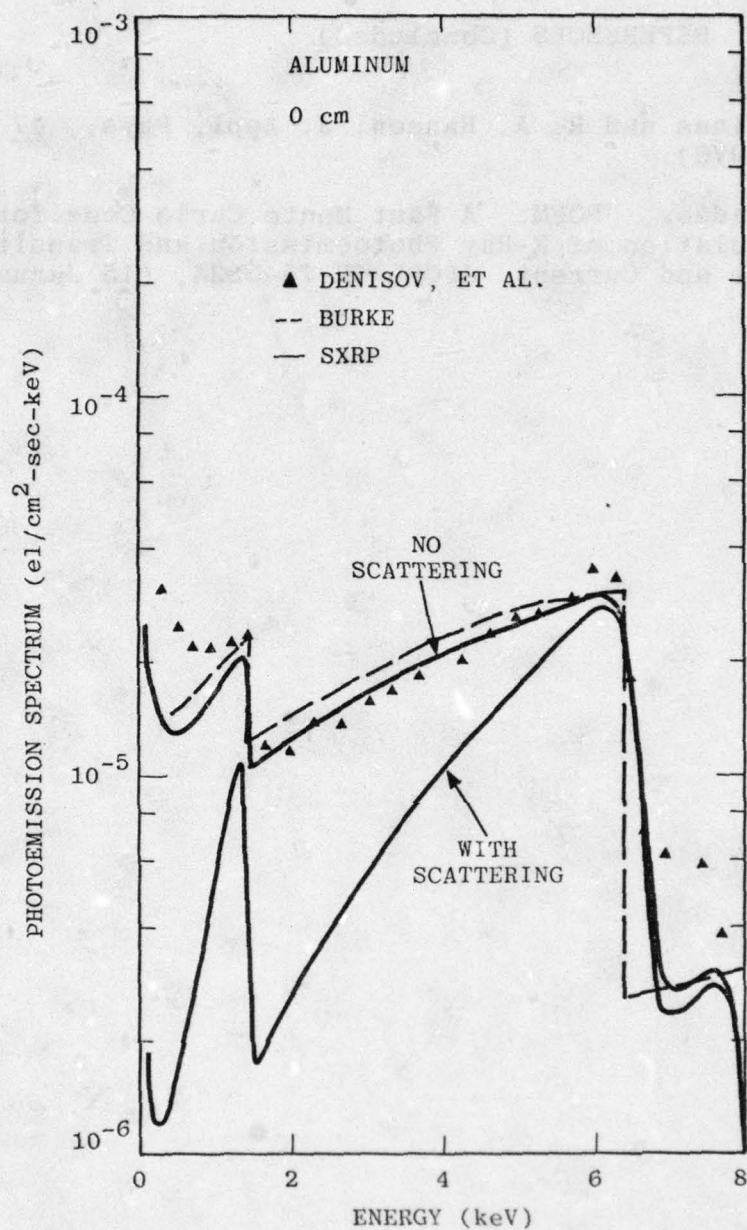


FIGURE 1. Photoemission Spectra for an 8 keV
Photon Source Incident on Al. The Solid
Curves are SXP Results With and Without Scattering

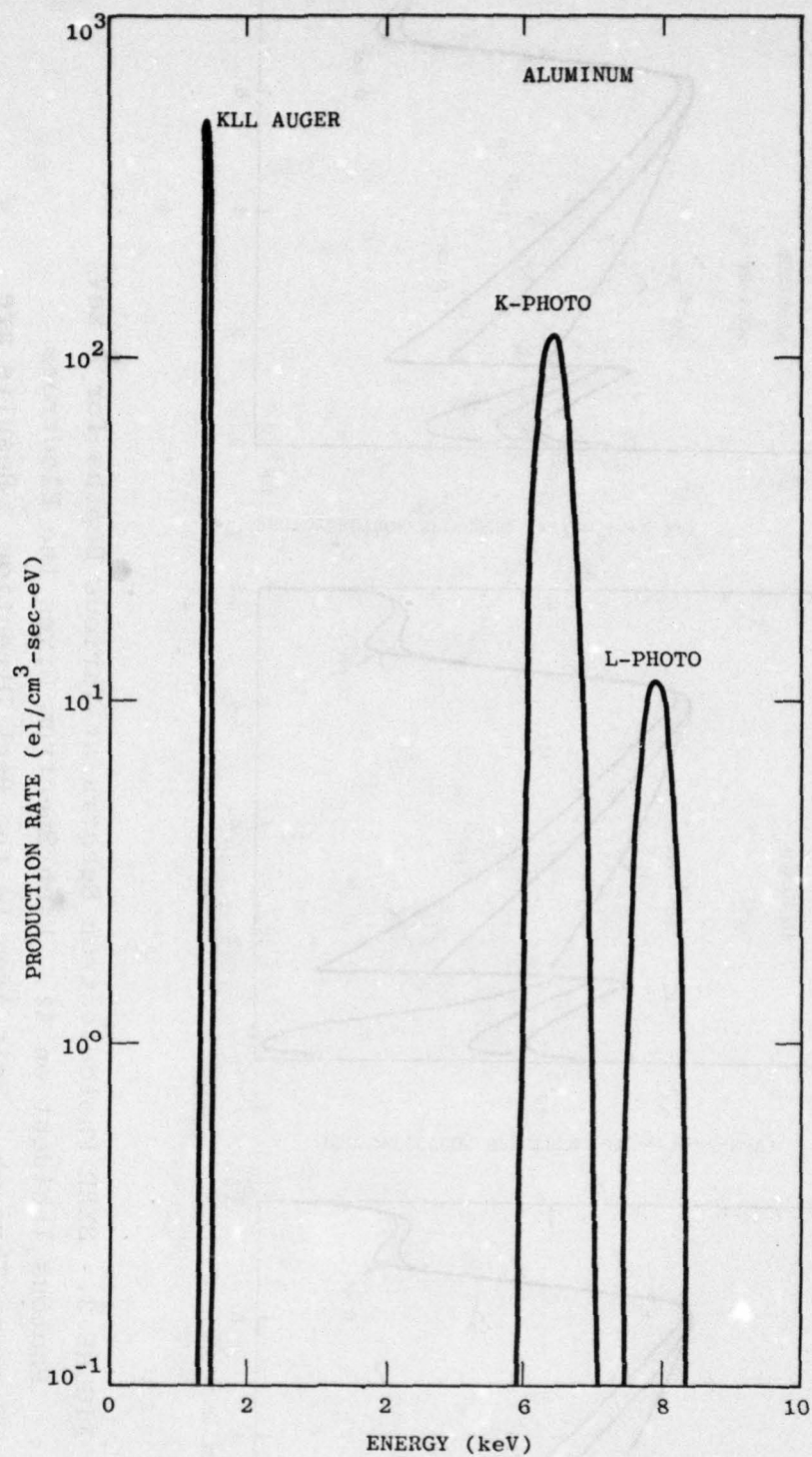


FIGURE 2. Source Distribution of Photo- and Auger Electrons for the 8 keV Gaussian Photon Source Used to Perform the SXRP Calculations

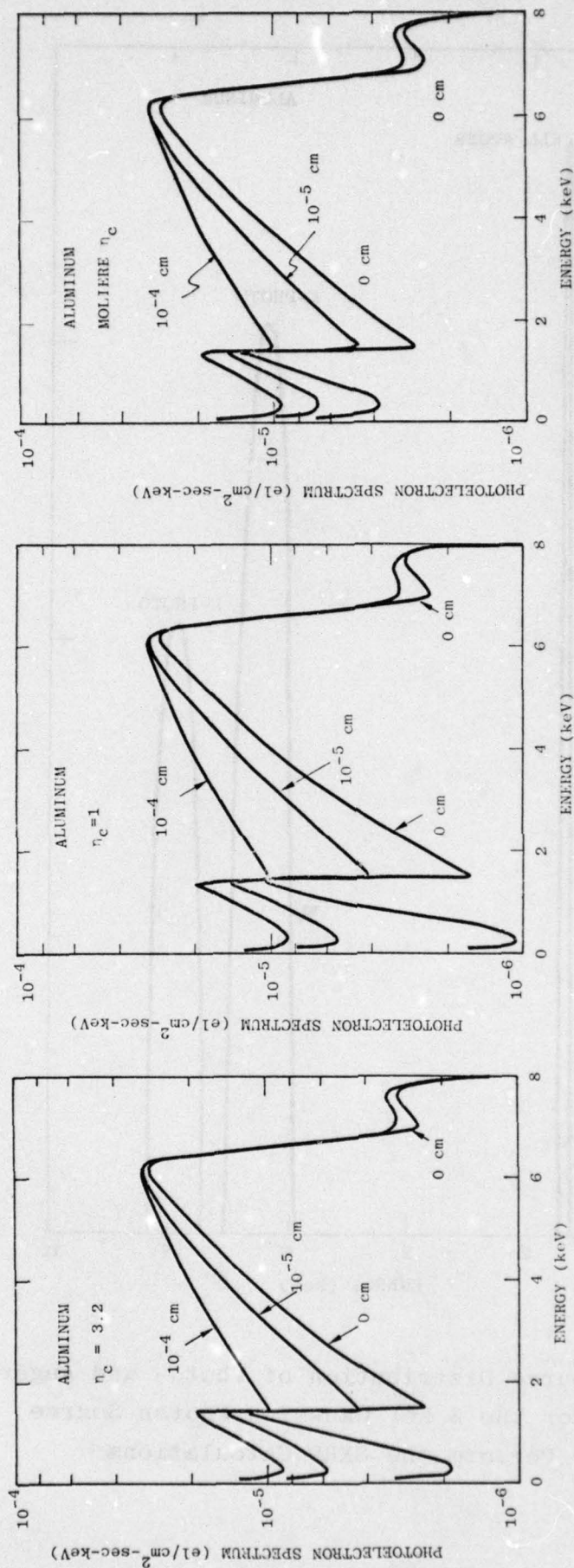


FIGURE 3. SXR Photoelectron Spectra at Various Depths for 8 keV Photons Incident on Al. Each Spectrum Gives the Electrons Passing Through a Unit Area in the Back Direction. Results are Shown for Three Different Representations of the Elastic Scattering IMFP Designated by η_c

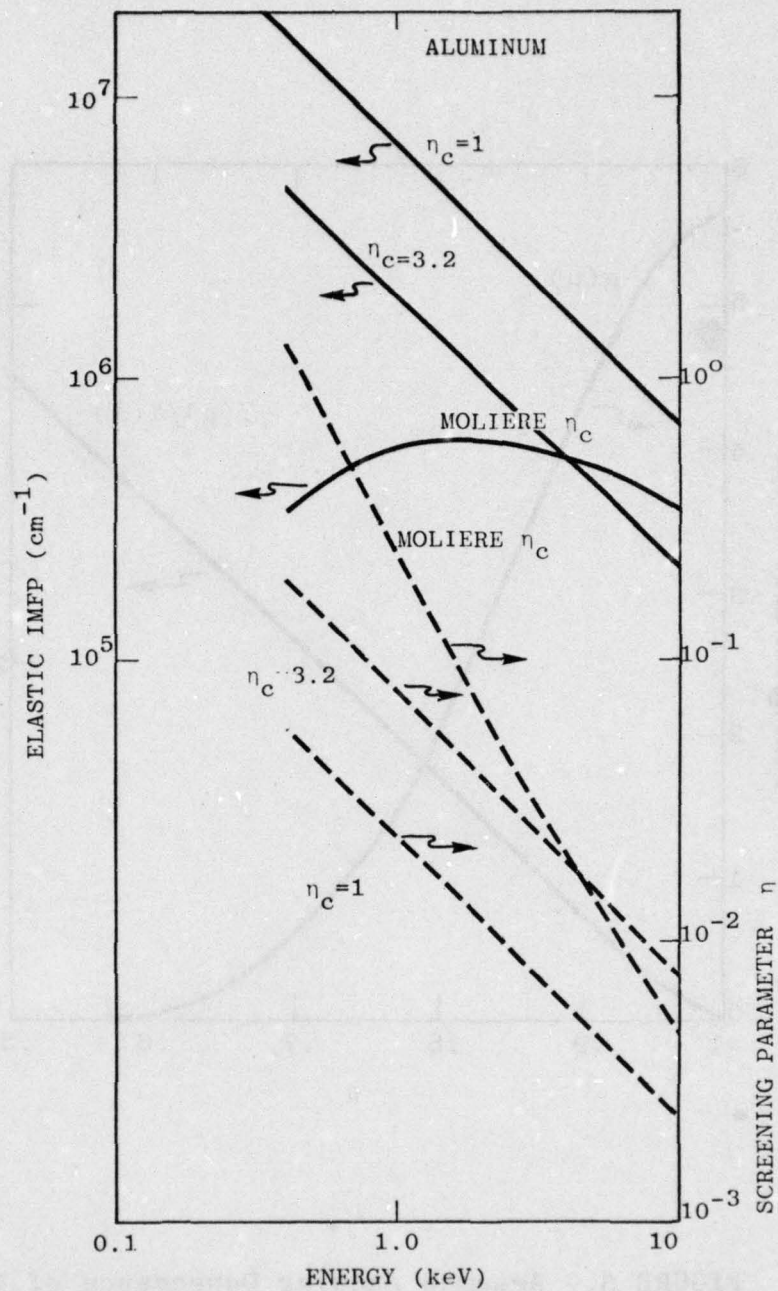


FIGURE 4. Energy Dependence of Screening Parameters and Corresponding Elastic IMFP's Used to Perform the Backscatter Calculations for Al

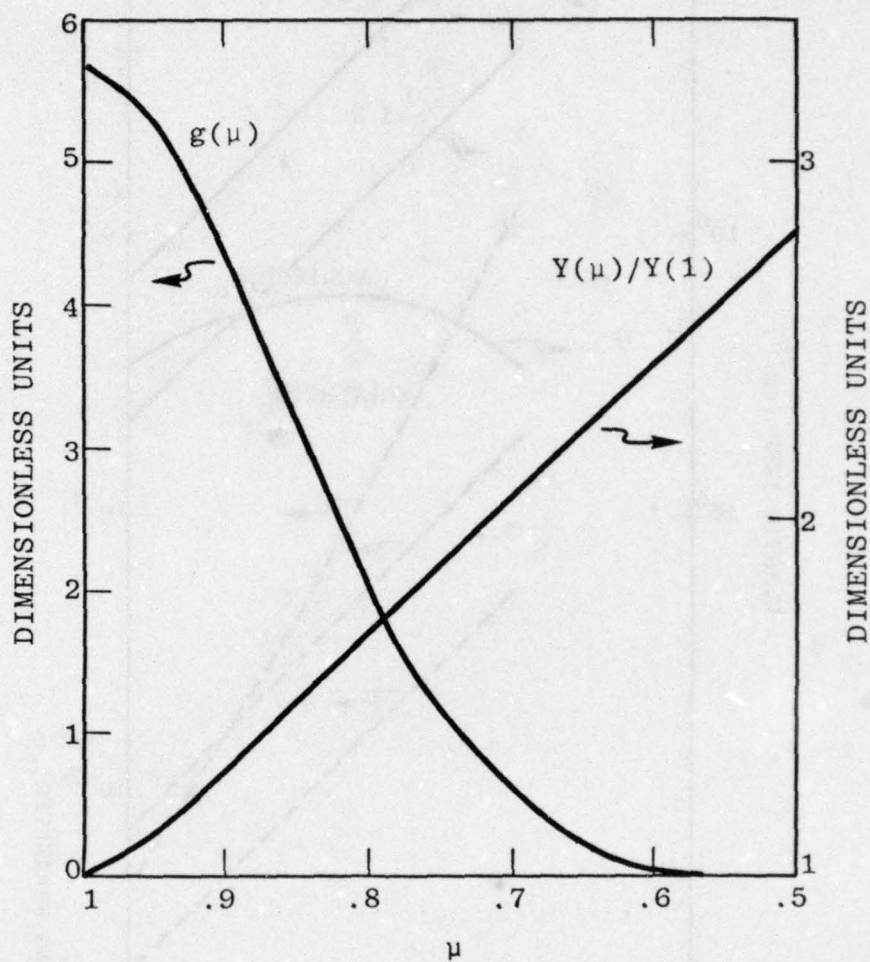


FIGURE 5. Assumed Angular Dependence of the Incident Electrons and the Backscatter Yield.
 μ is the Cosine of the Incidence Angle

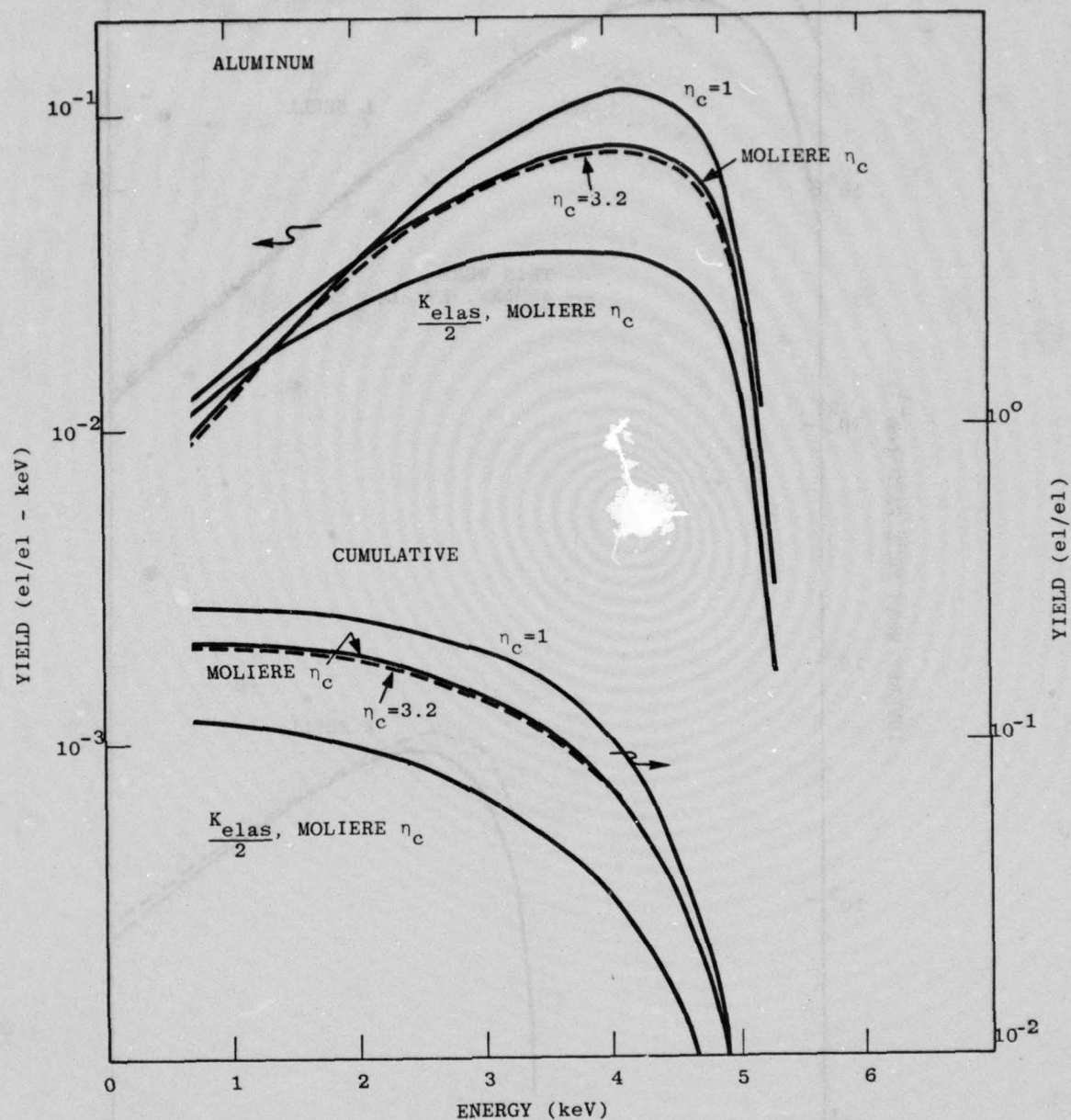


FIGURE 6. Differential and Cumulative Backscatter Yields for the Various Representations of the Elastic Scattering Cross Sections Described in the Text

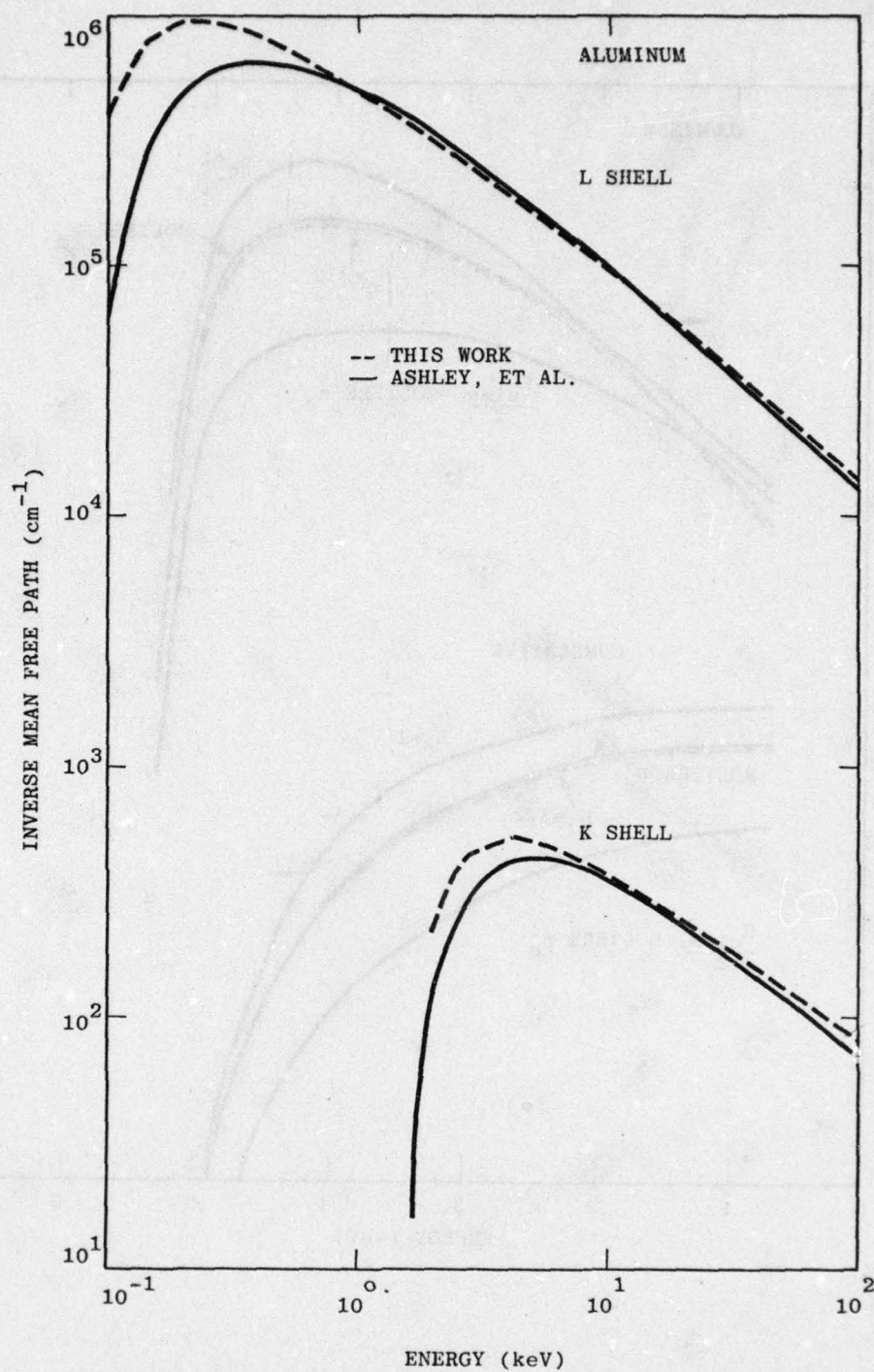


FIGURE 7. A Comparison of Inner Shell IMFP's Given by Integrating Equation (10) and by Ashley, et al.¹¹ from more rigorous calculations

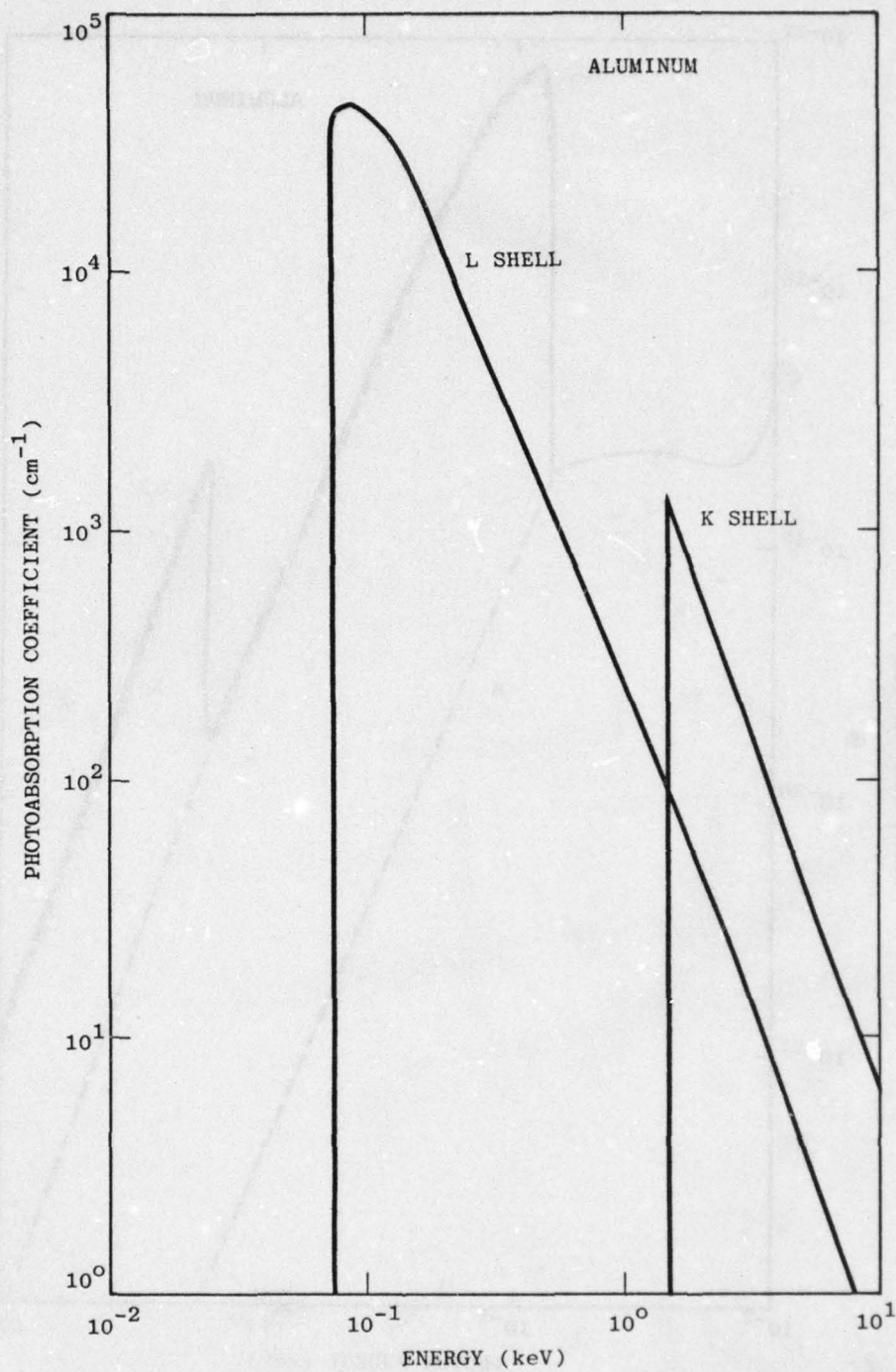


FIGURE 8. The Photoabsorption Coefficients Used to Calculate the IMFP's shown in Figure 7

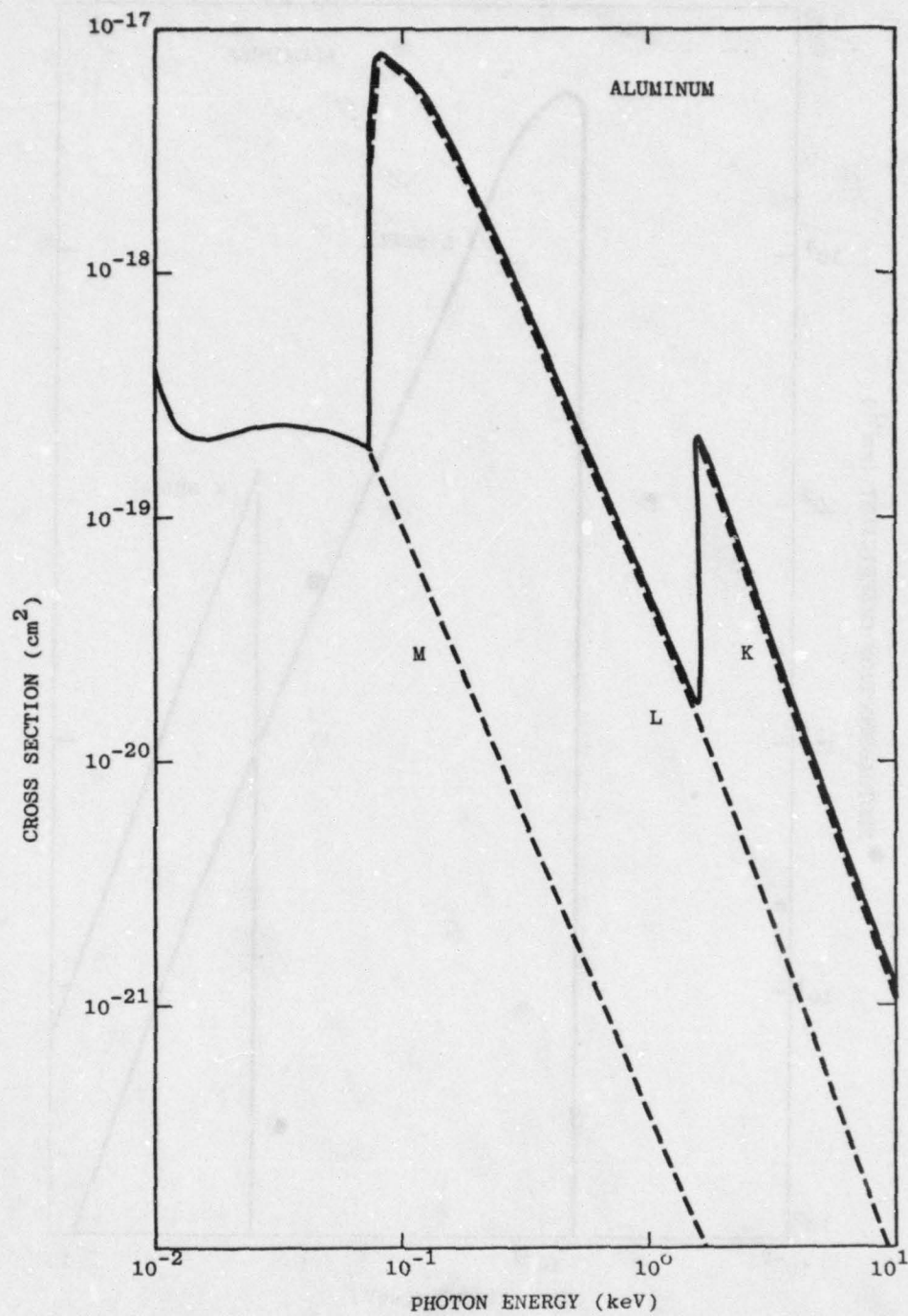


FIGURE 9. Photoabsorption Cross Sections for Al

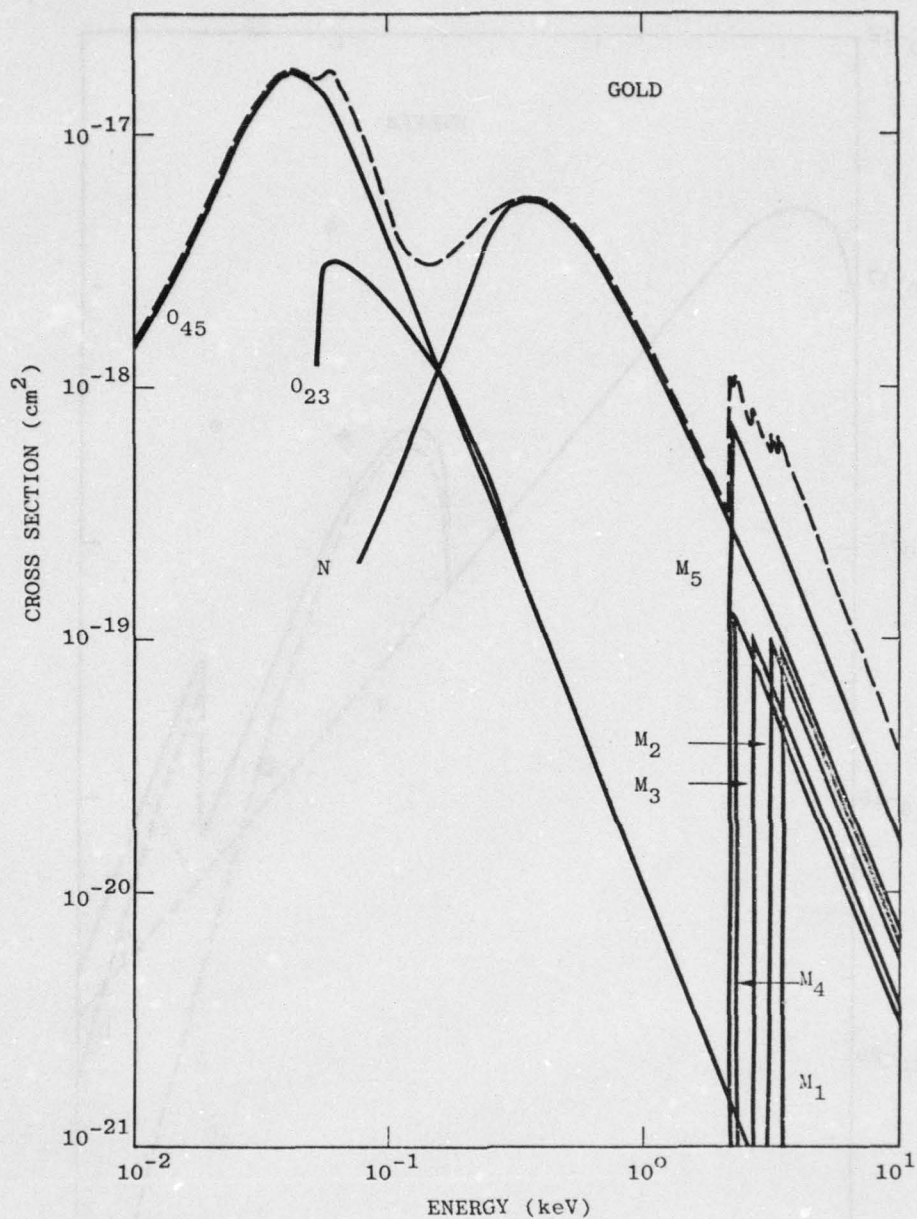


FIGURE 10. Photoabsorption Cross Sections for Au

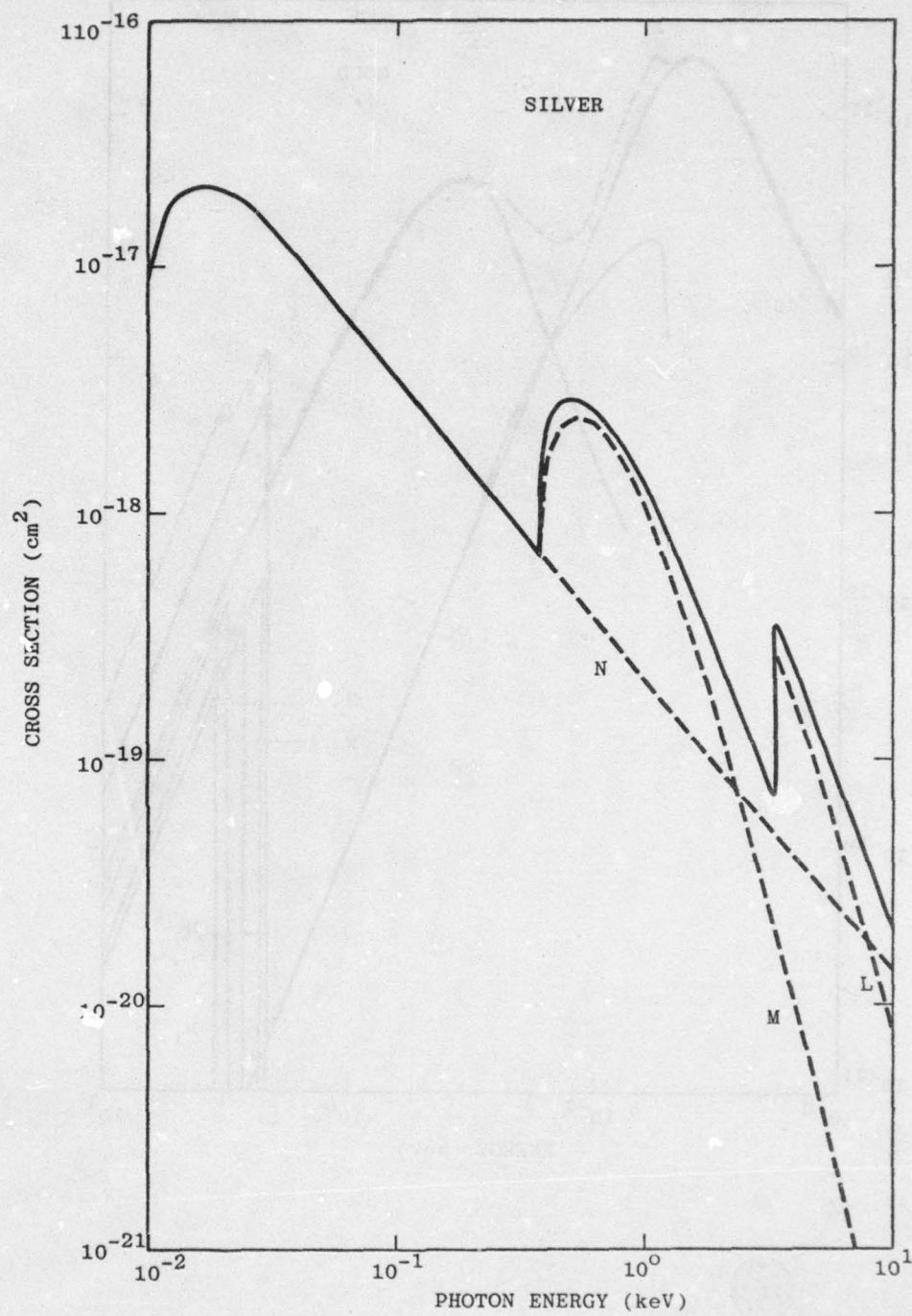


FIGURE 11. Photoabsorption Cross Sections for Ag

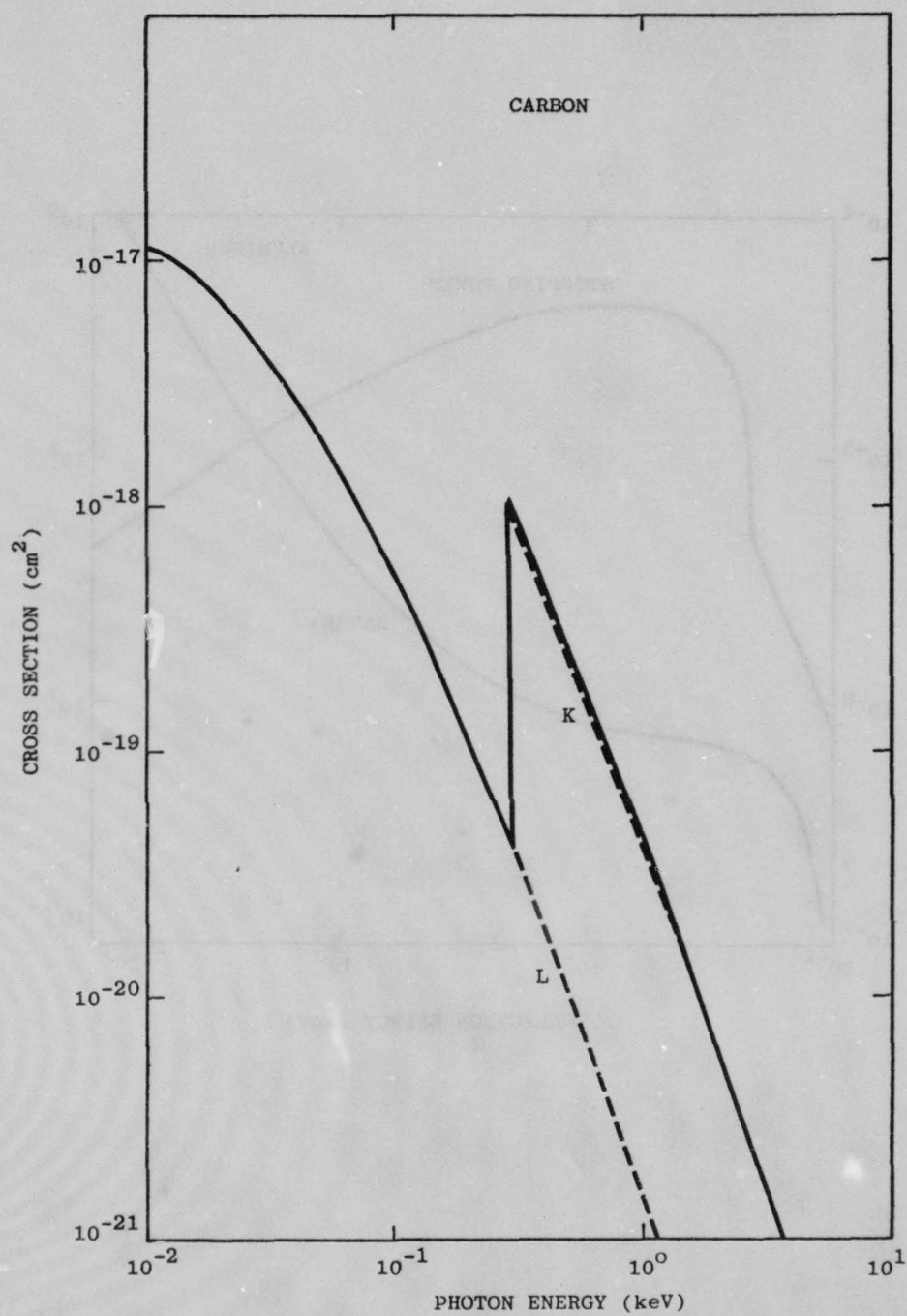


FIGURE 12. Photoabsorption Cross Sections for C

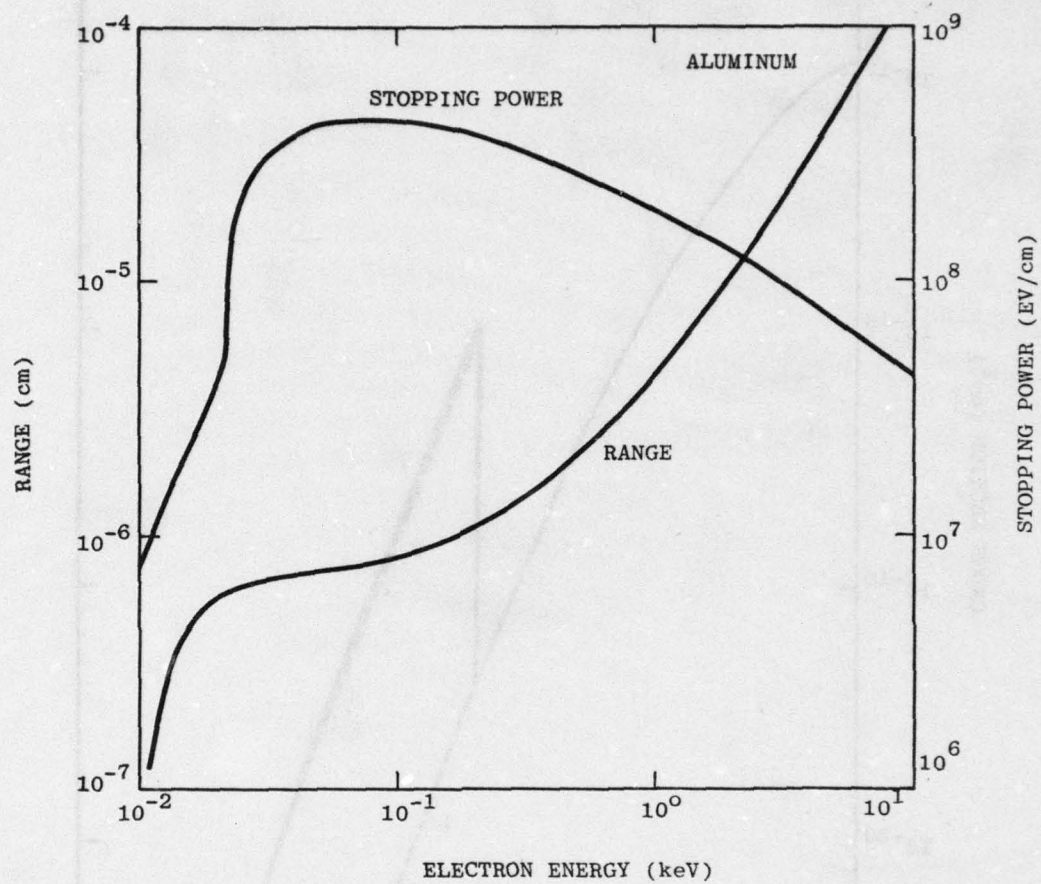


FIGURE 13. Range and Stopping Power for Al

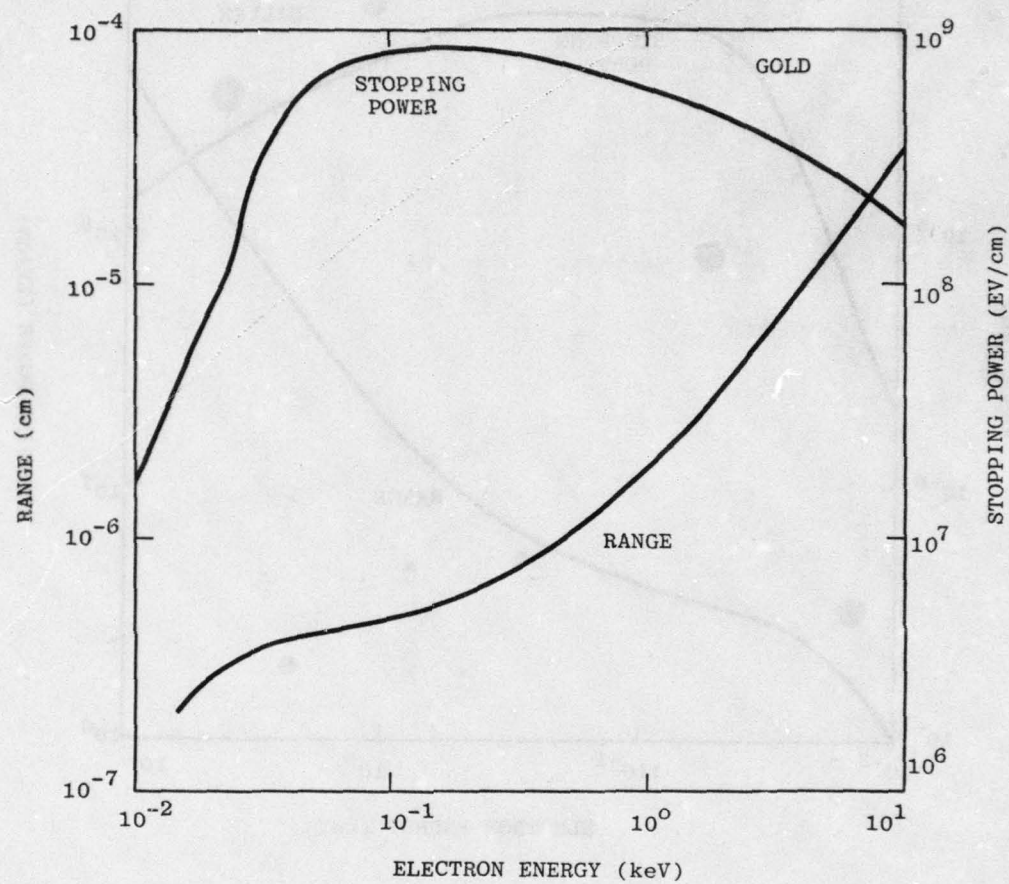


FIGURE 14. Range and Stopping Power for Au

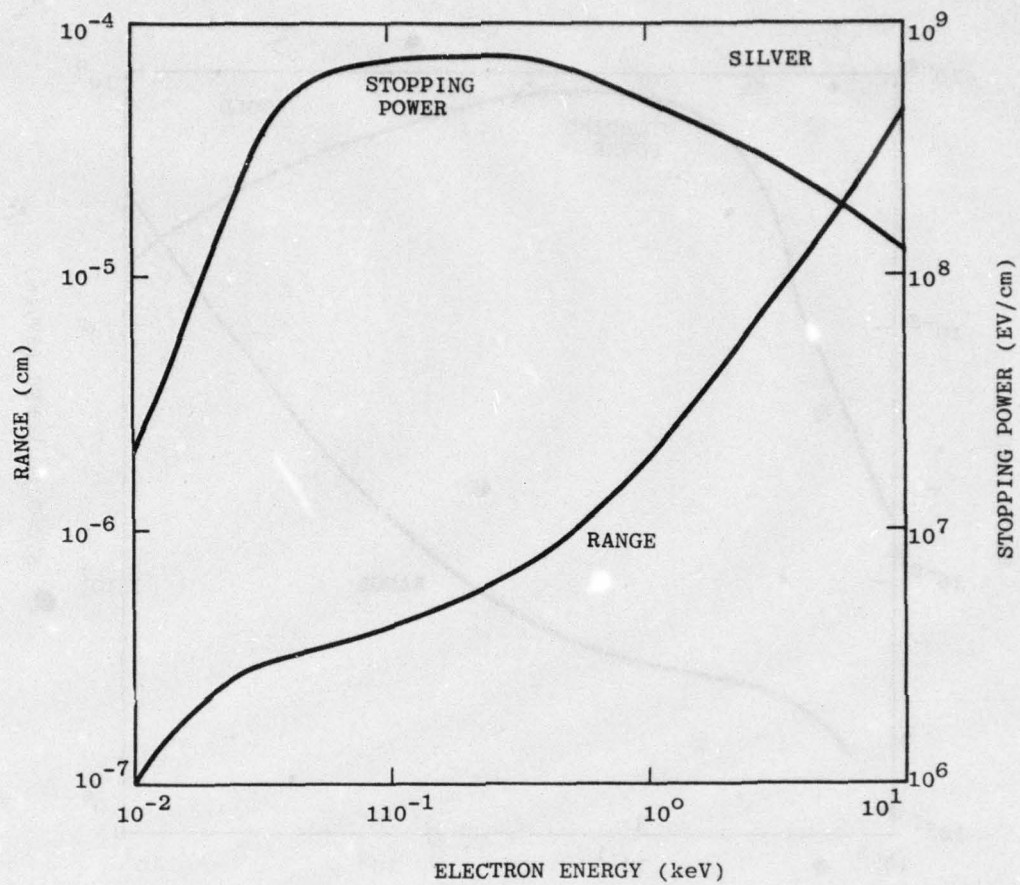


FIGURE 15. Range and Stopping Power for Ag

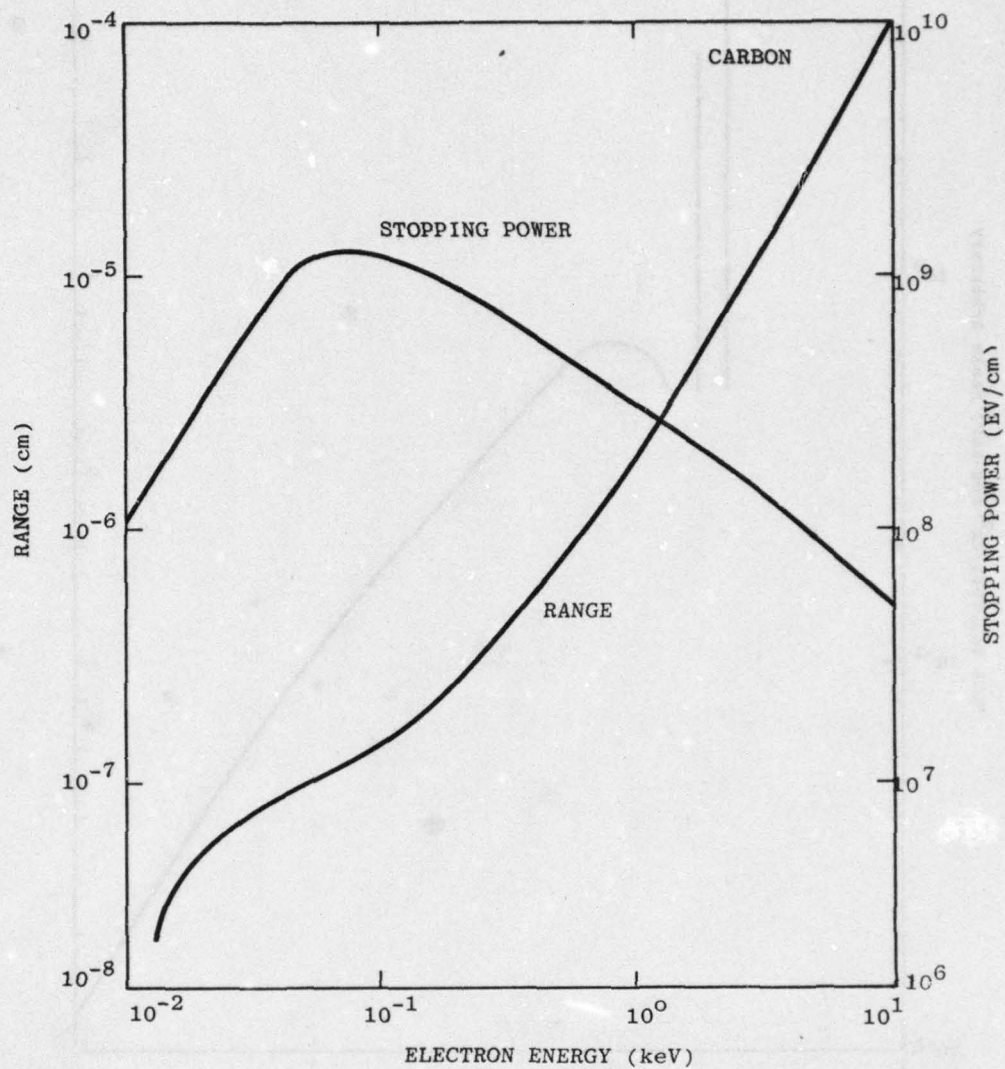


FIGURE 16. Range and Stopping Power for C

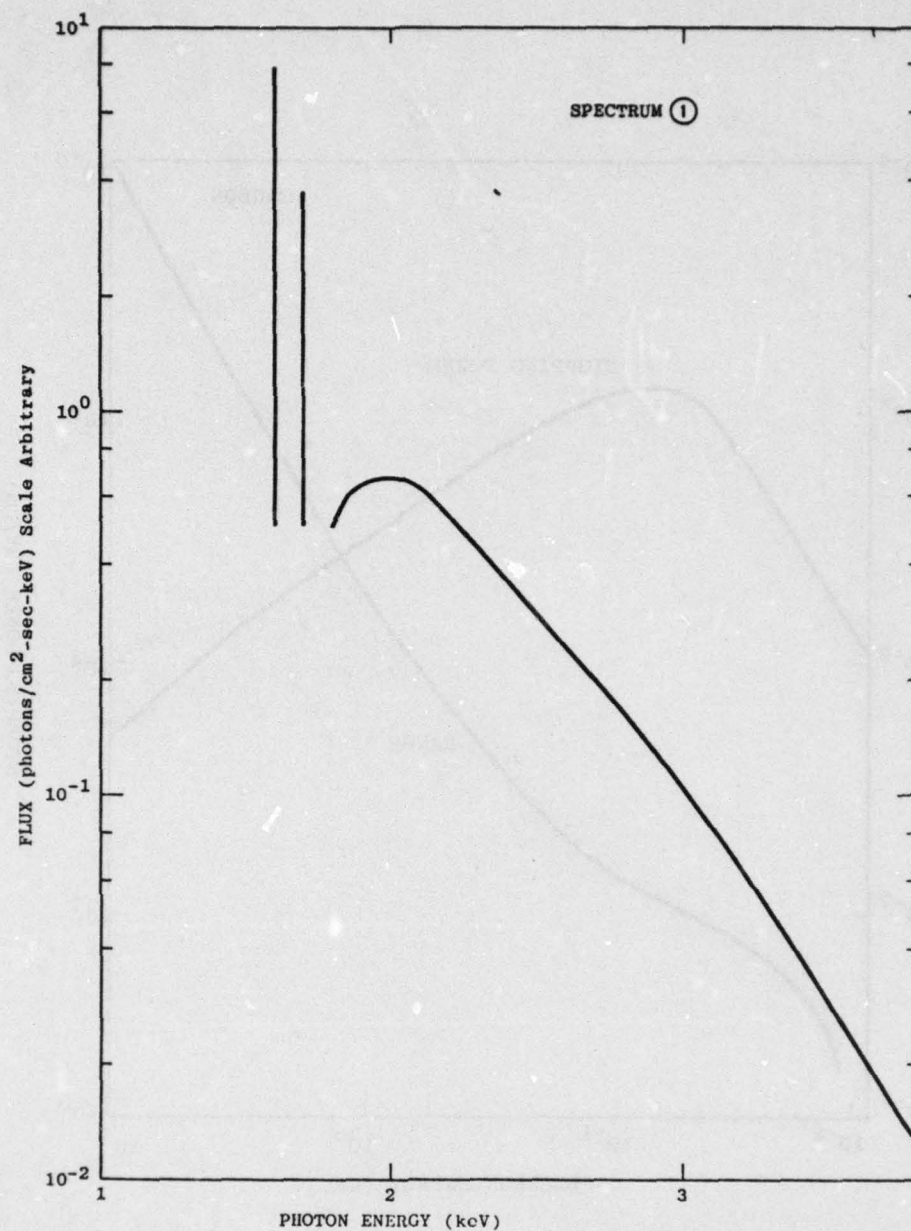


FIGURE 17. The First of Four Photon Spectra Used
to Study the Sensitivity of Photoemission
to Variations in the EWR Source

Approximately 50% of the photon
energy is contained in the two lines.

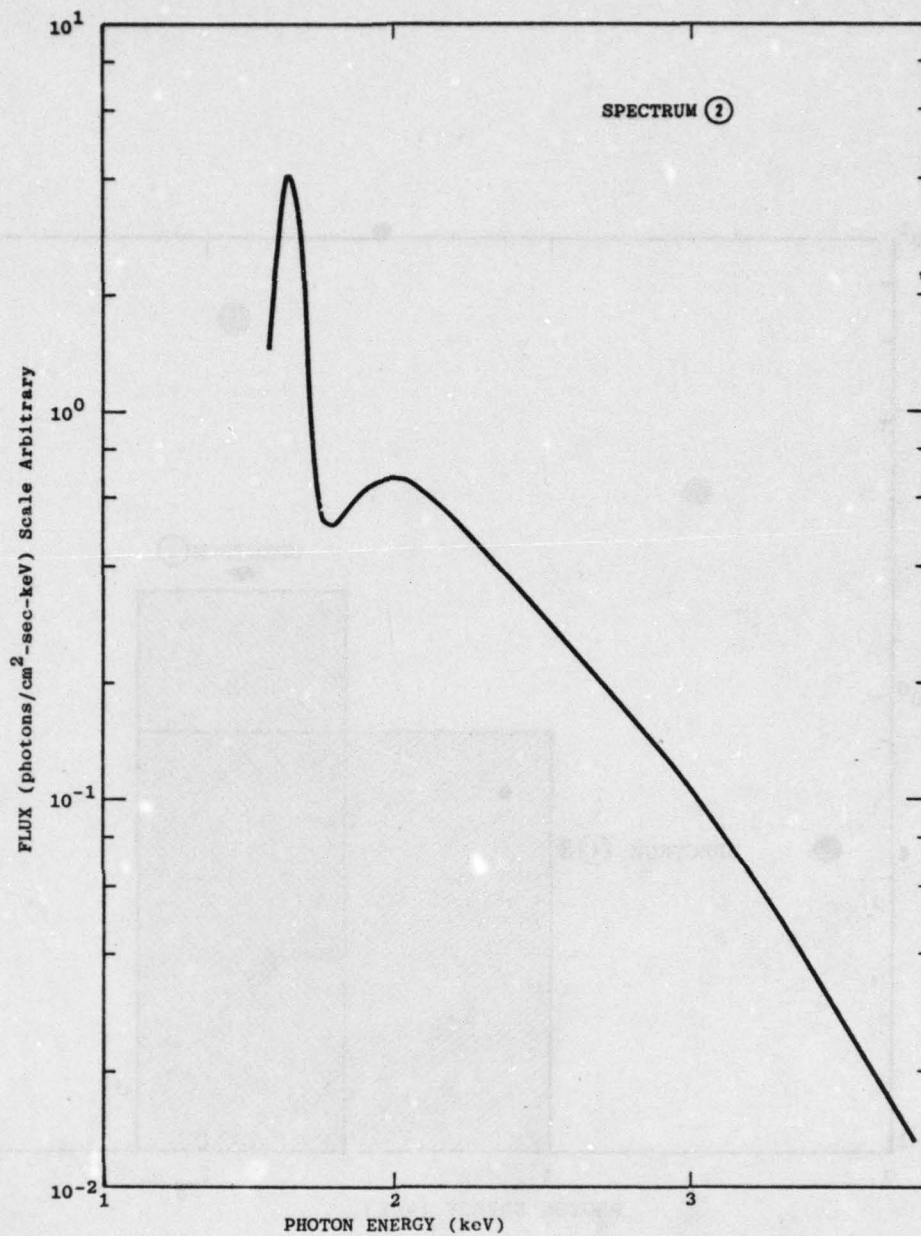


FIGURE 18. The Second of Four
Photon Spectra Considered

The Gaussian feature centered at 1.6 keV
contains ~50% of the photon energy and is used
as a continuum approximation for the
two lines in spectrum ①.

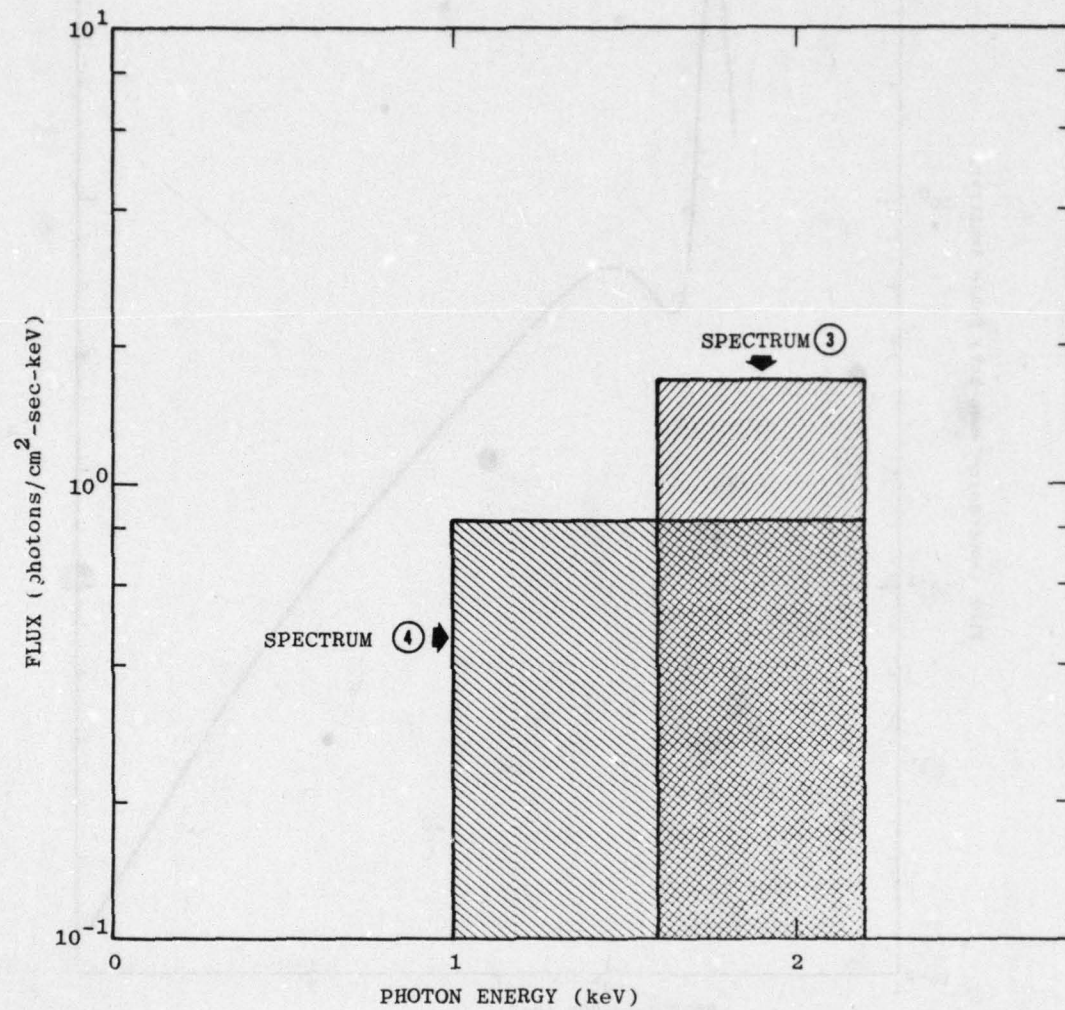


FIGURE 19. The Remaining Two Photon Spectra for Performing the Sensitivity Analysis

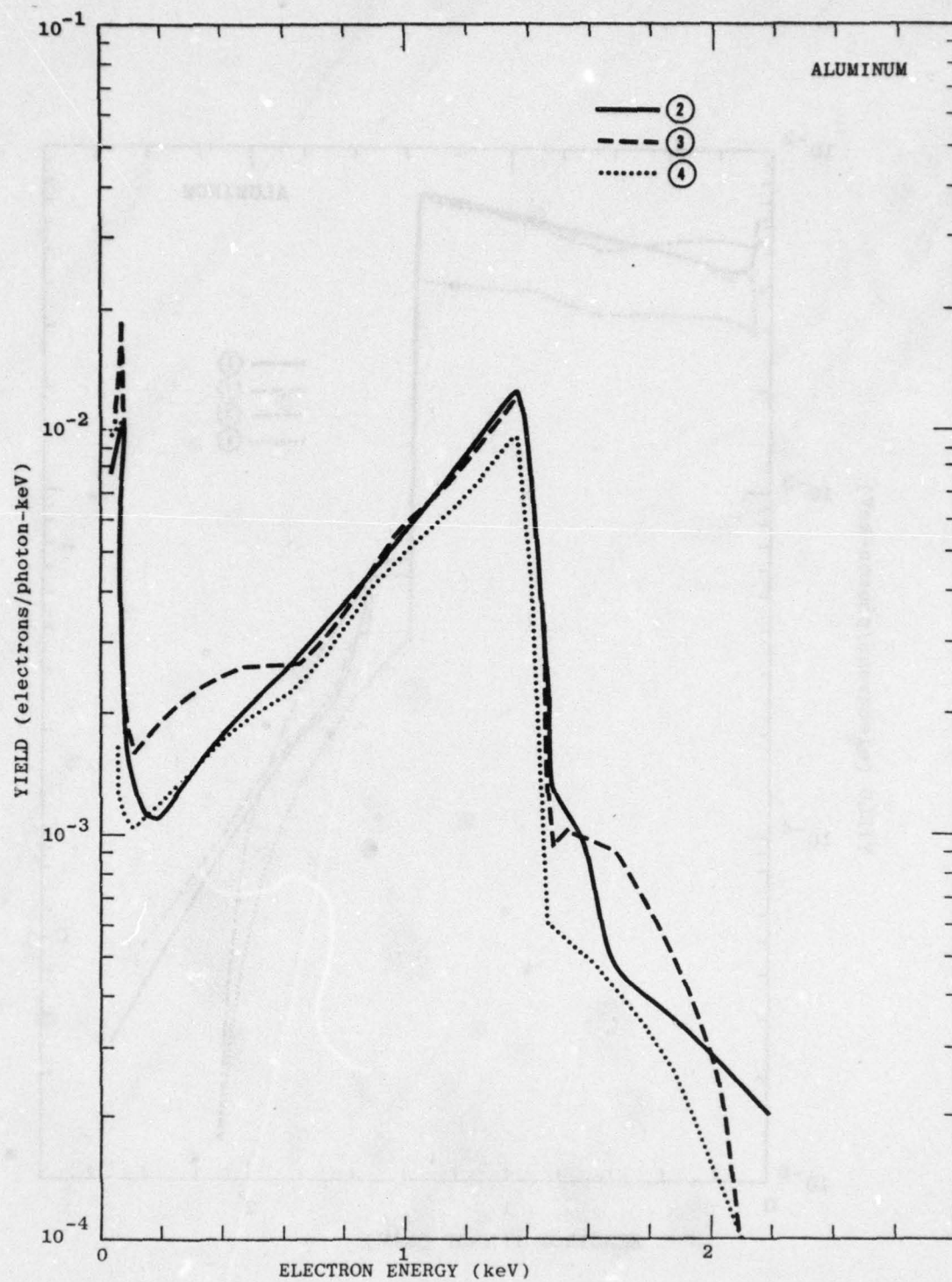


FIGURE 20. Differential Yields for Al Obtained with the Transport Code for Photon Spectra (2)-(4)

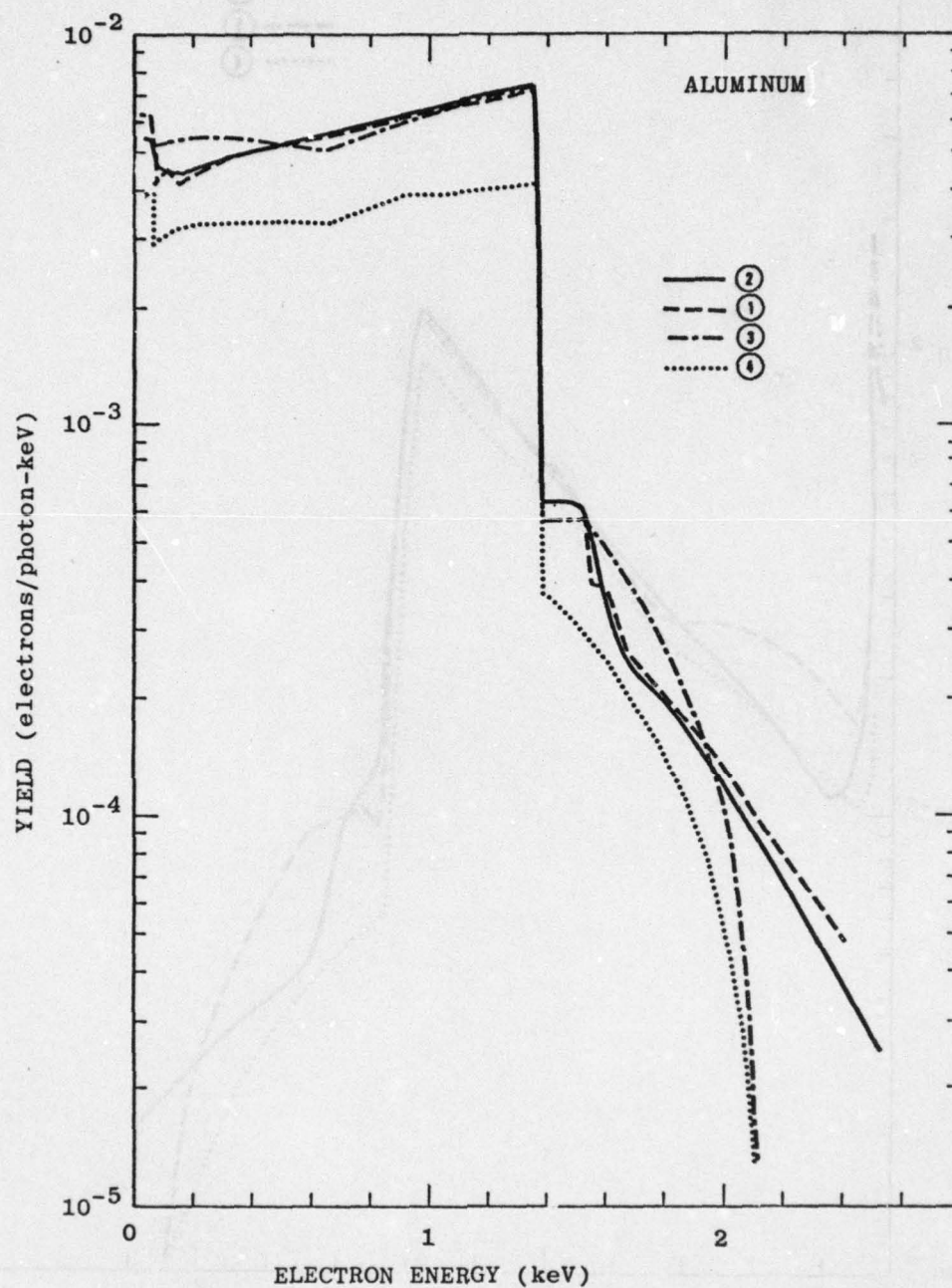


FIGURE 21. Empirical Differential Yields for Al
for Photon Spectra ①-④

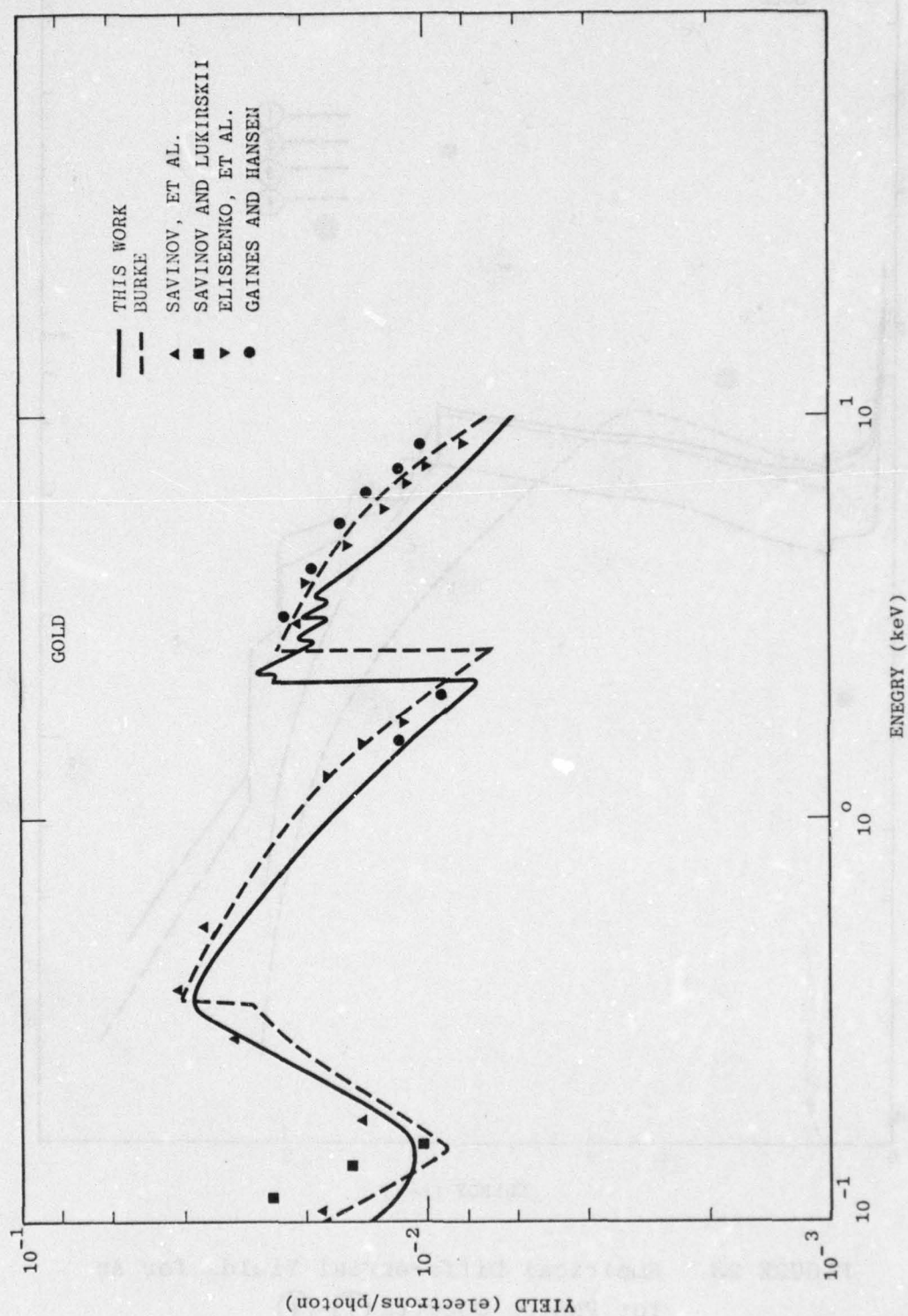


FIGURE 22. Empirical Total Yields versus Photon Energy for Au

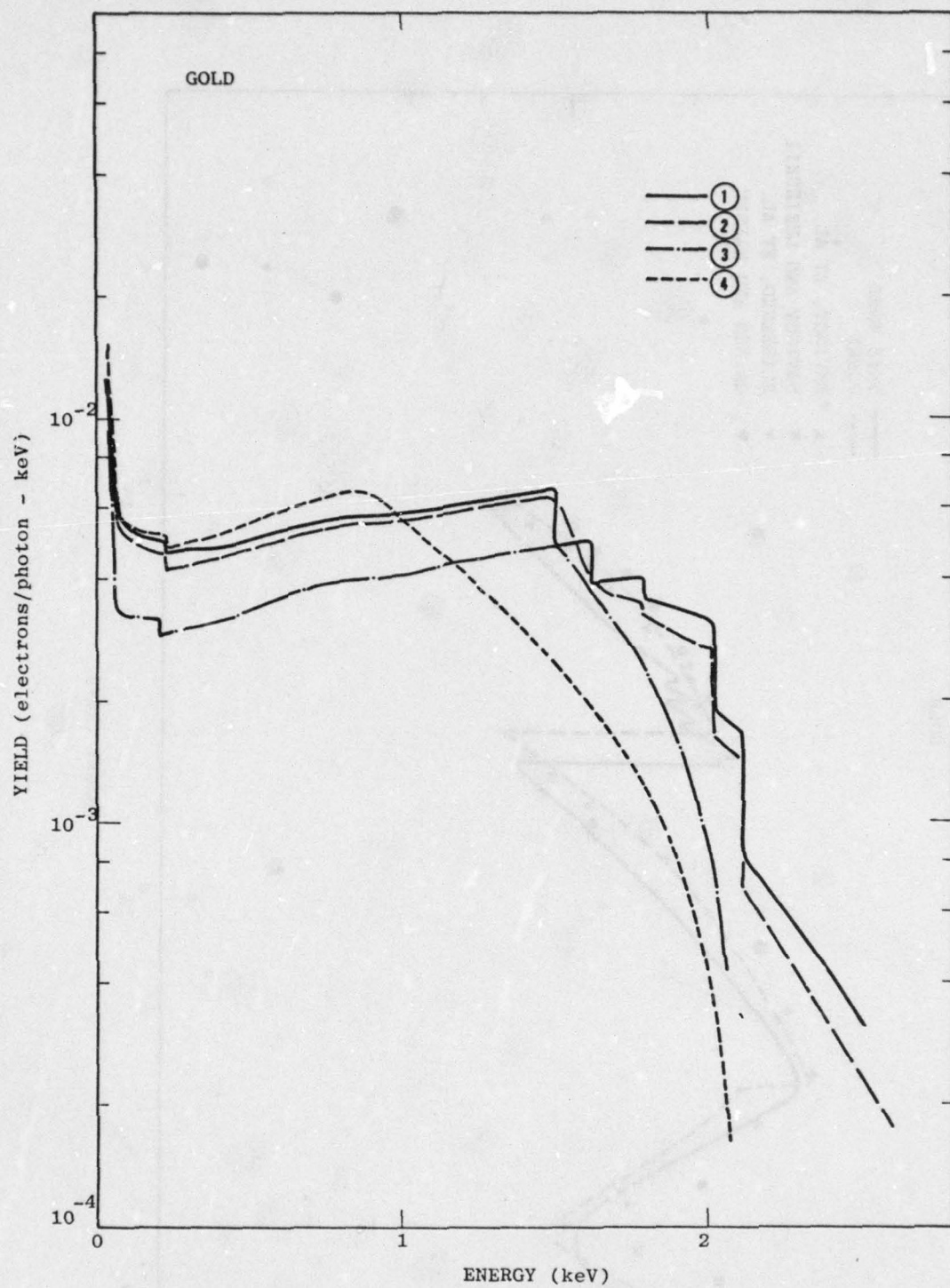


FIGURE 23. Empirical Differential Yields for Au
for Photon Spectra ①-④

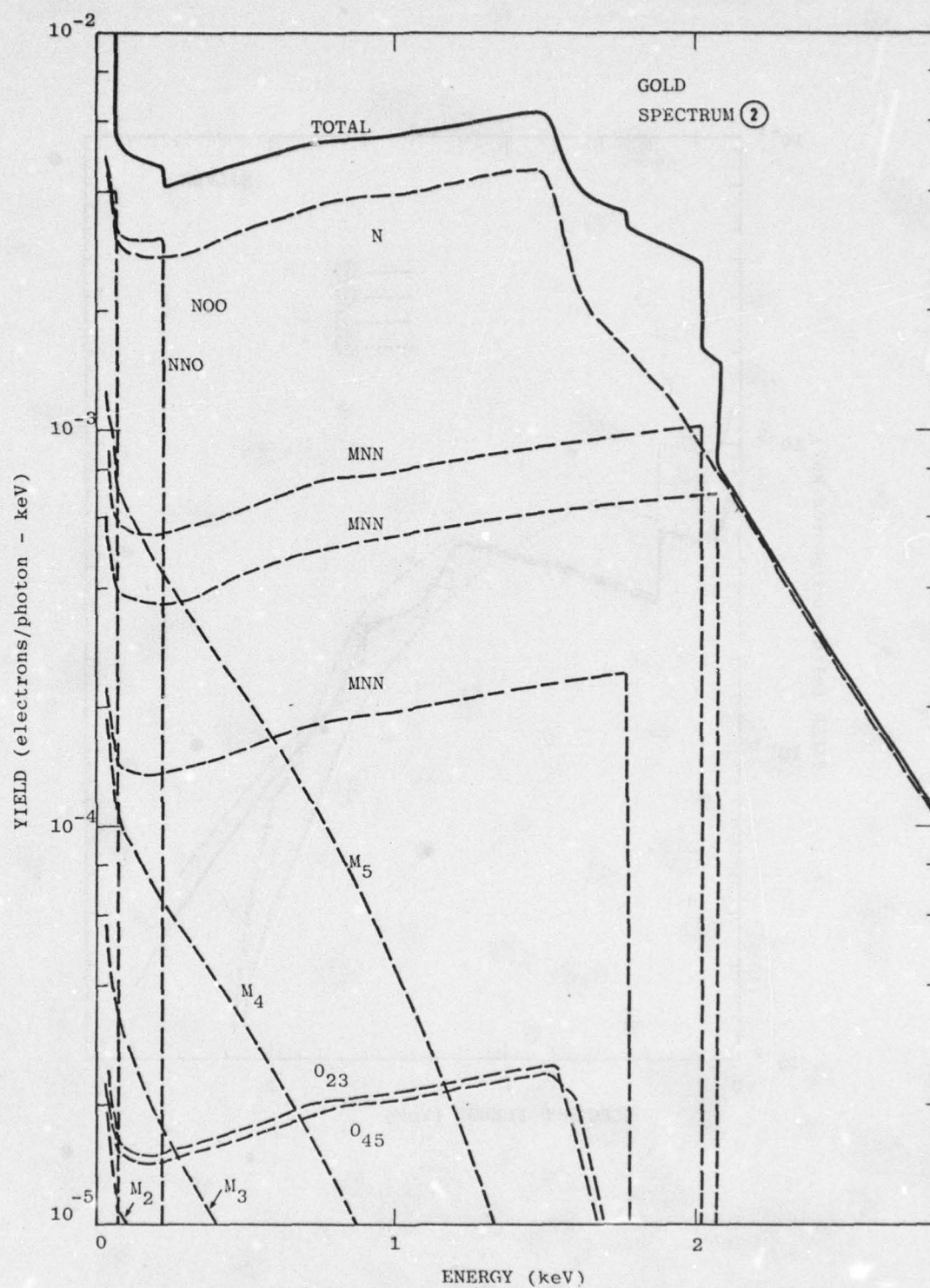


FIGURE 24. Empirical Differential Yield Components for Au for Photon Spectrum ②

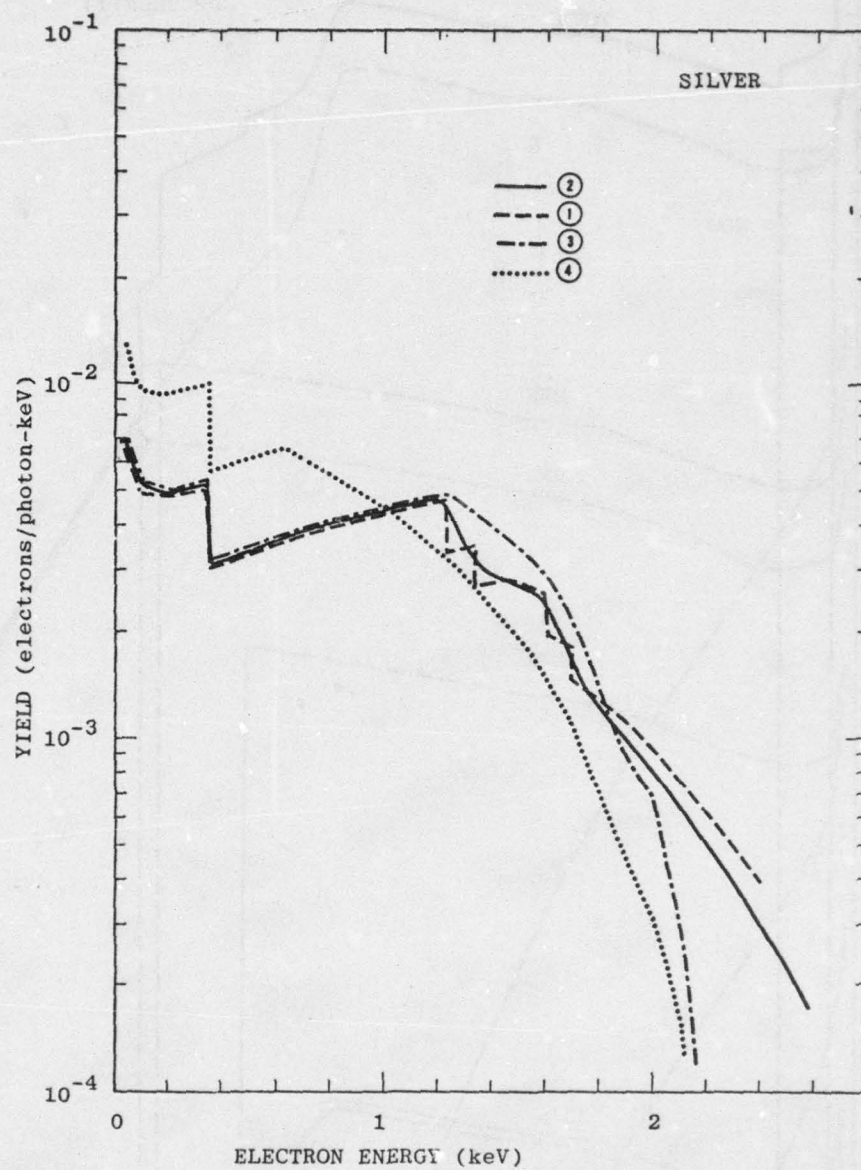


FIGURE 25. Empirical Differential Yields for Ag for Photon Spectra (1)-(4)

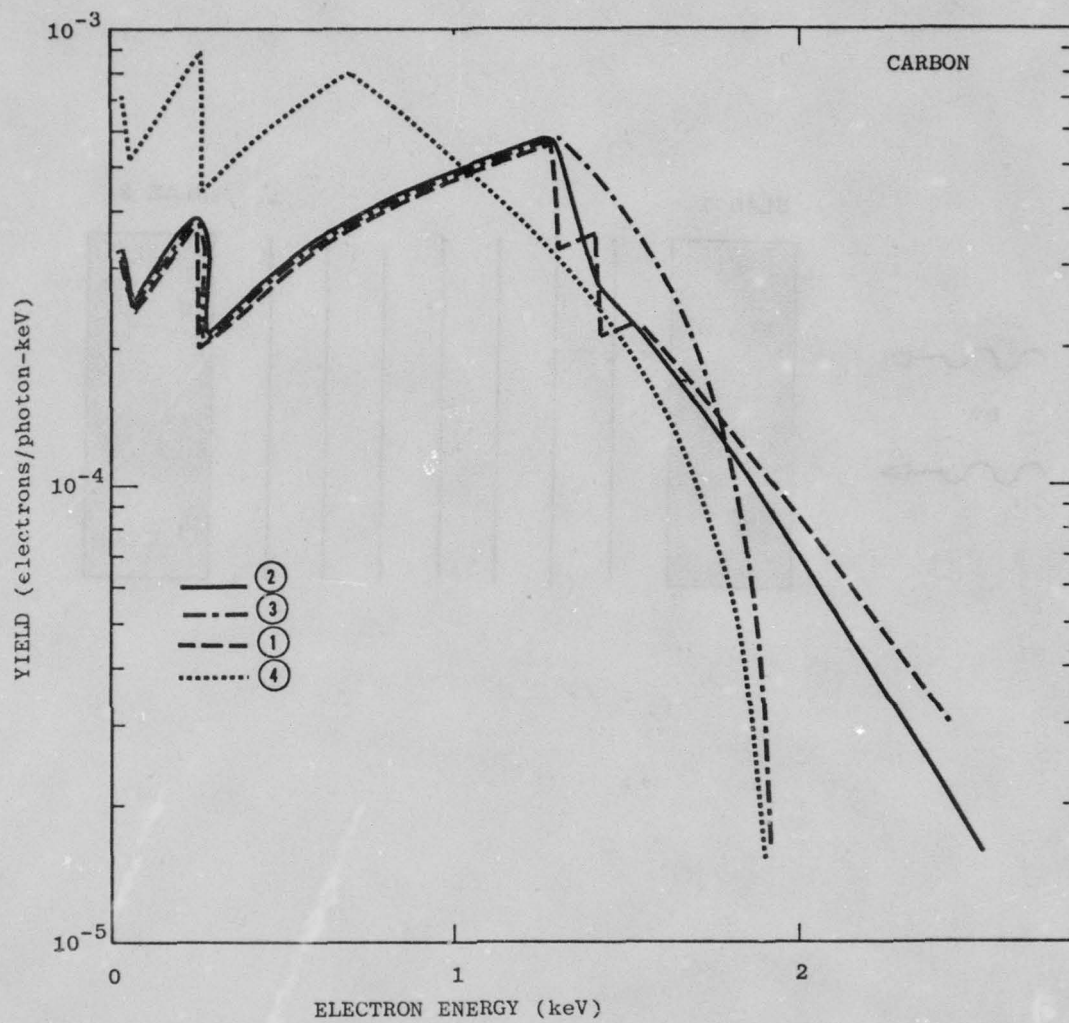


FIGURE 26. Empirical Differential Yields for C
for Photon Spectra ①-④

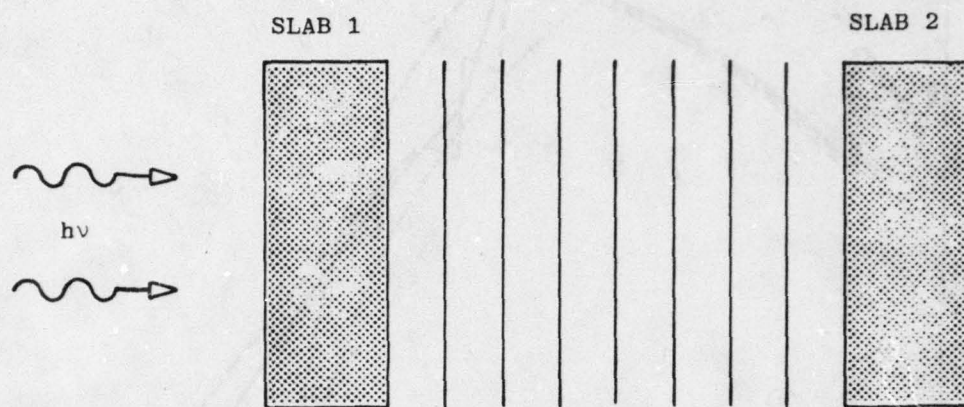


FIGURE 27. Transport Geometry

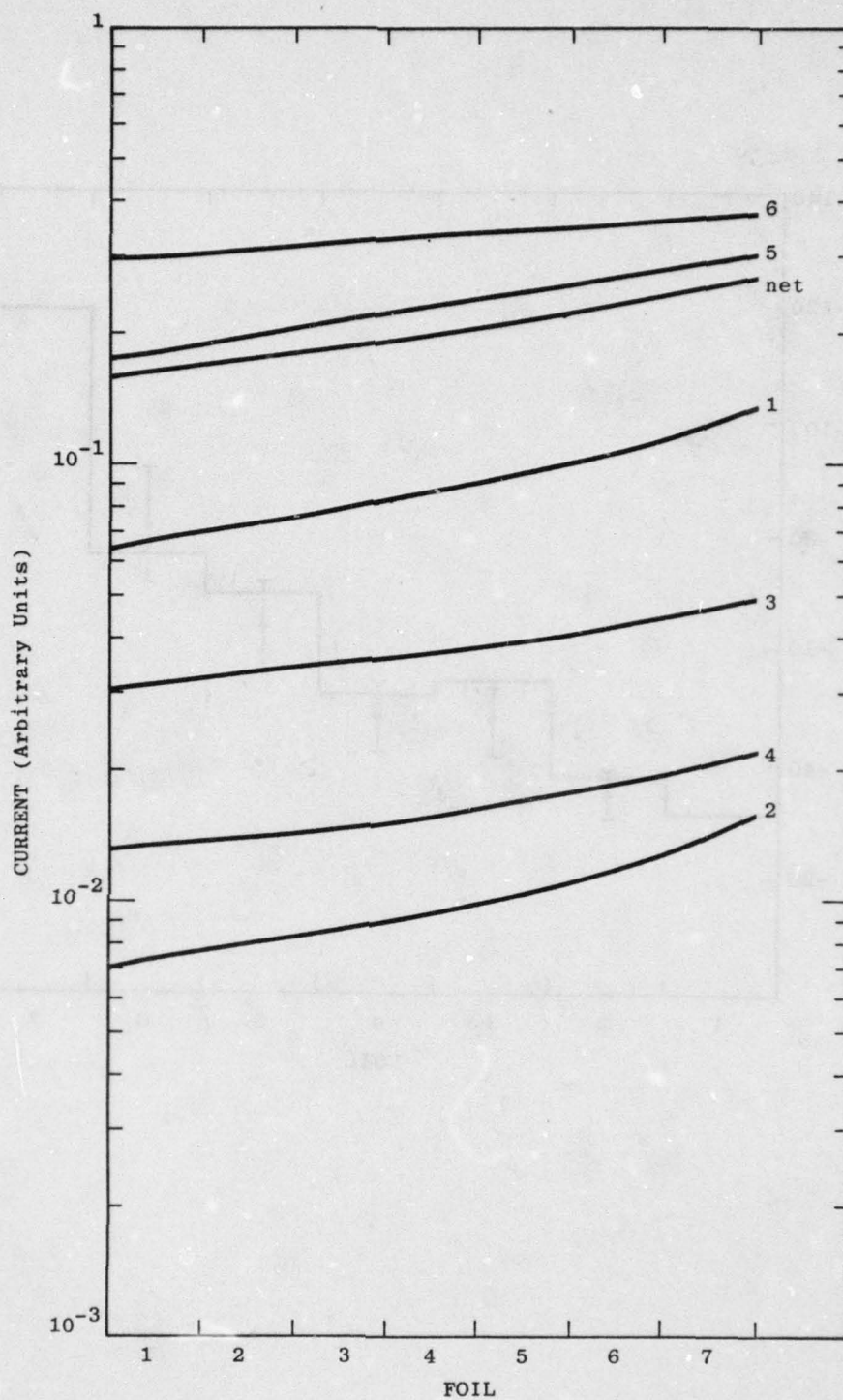


FIGURE 23. Currents in the foils for the
Al/Al/Pb Configuration

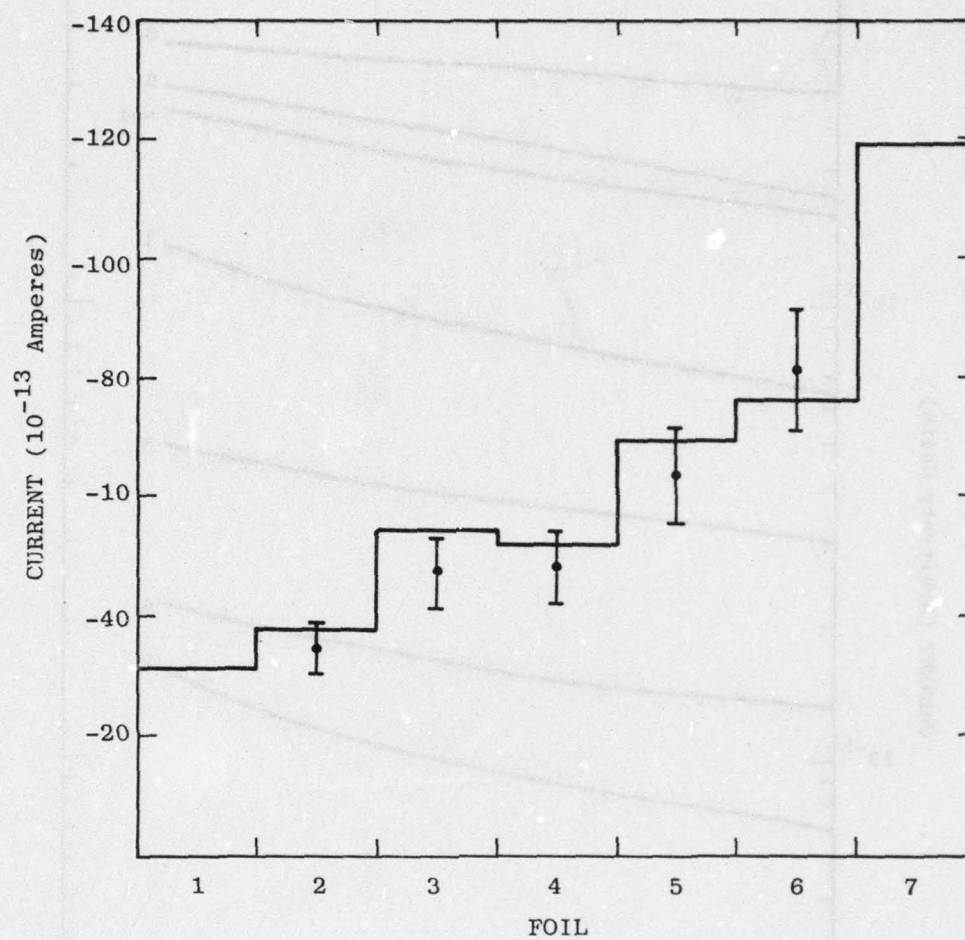


FIGURE 29. Charge Deposition Profile for the Al/Al/Pb Configuration

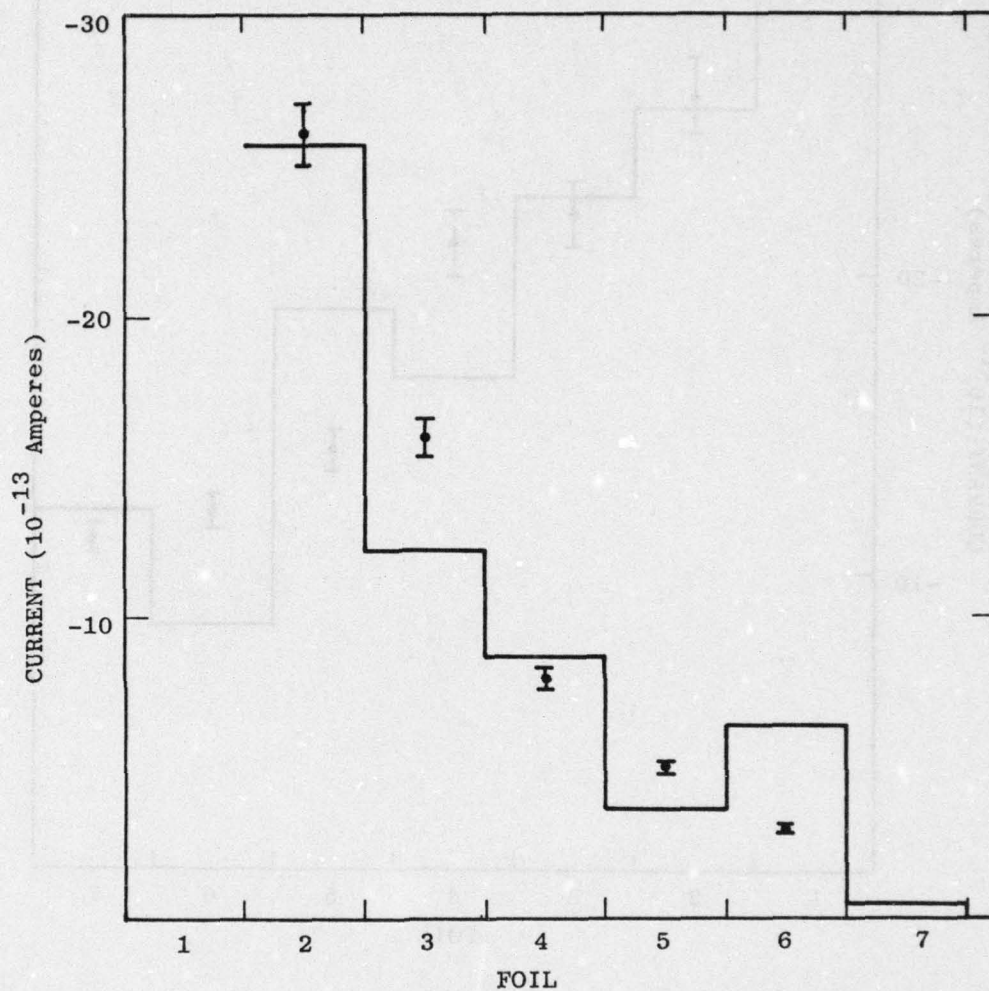


FIGURE 30. Charge Deposition Profile for the Pb/Al/Al Configuration

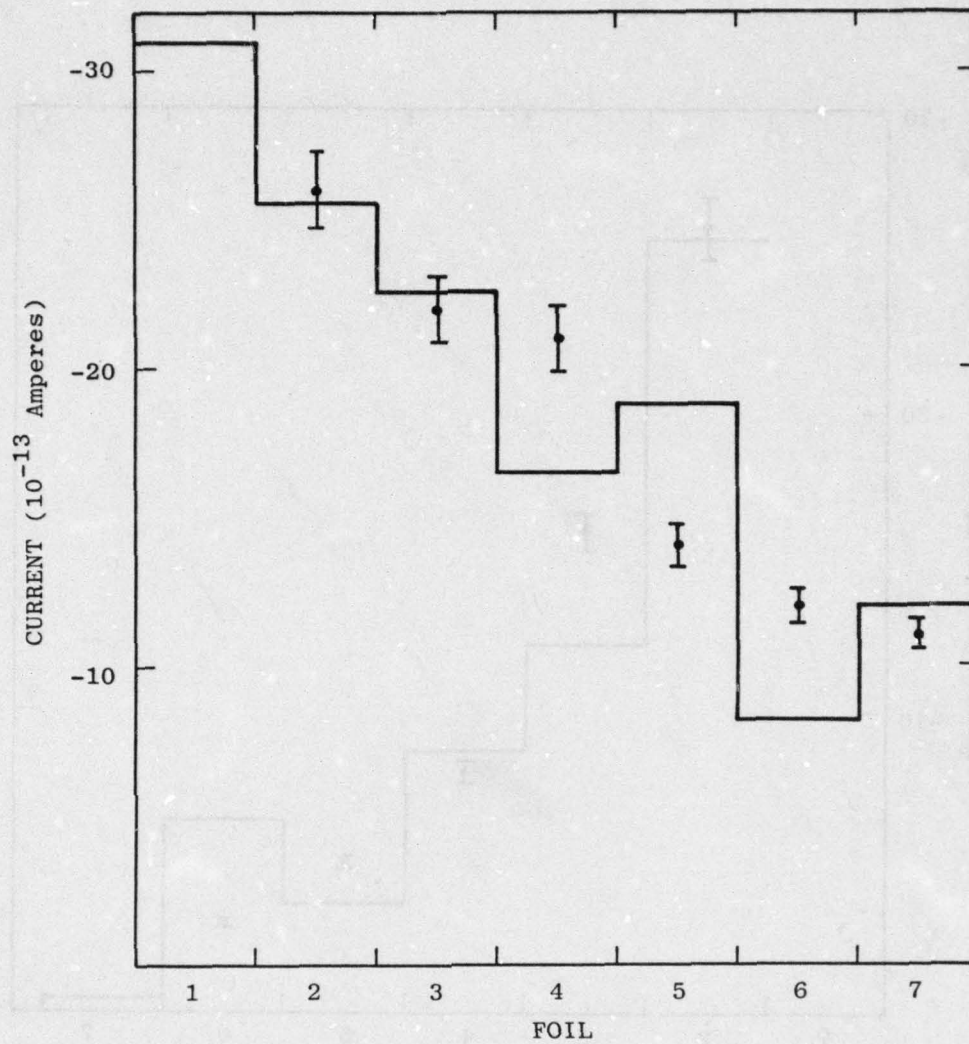


FIGURE 31. Charge Deposition Profile for the Pb/Sn/Sn Configuration

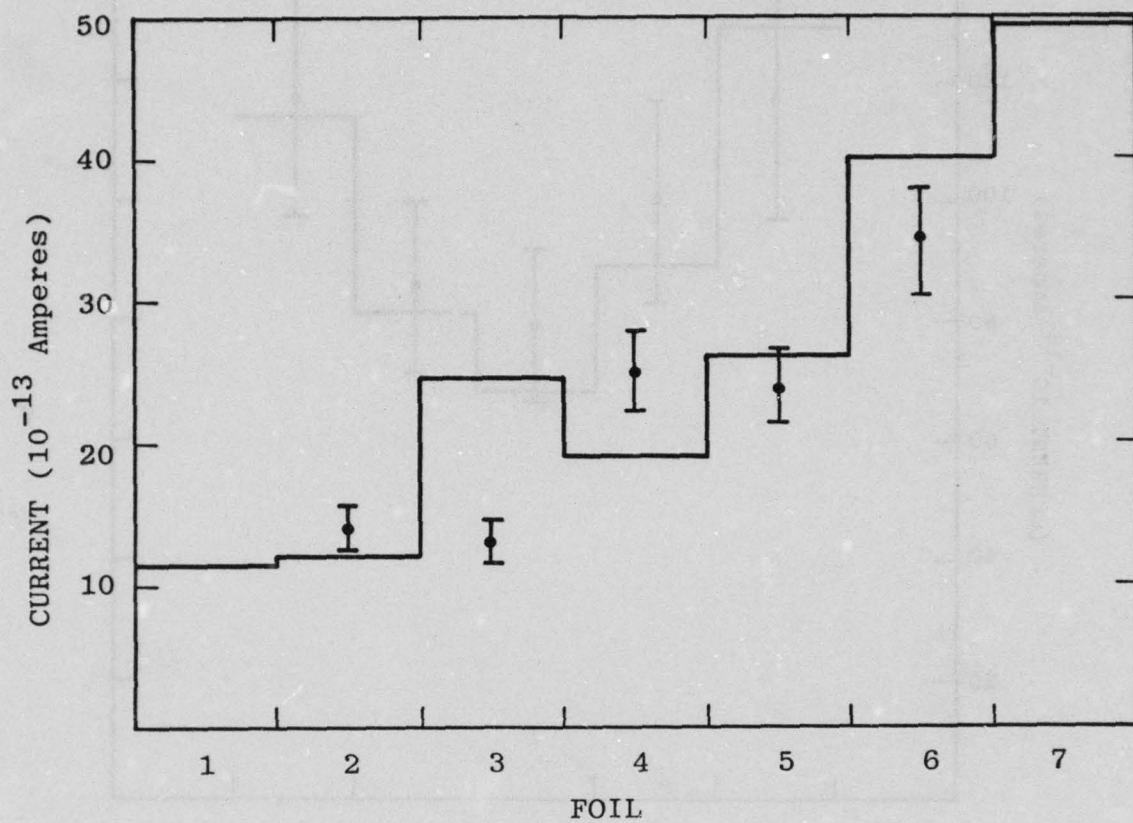


FIGURE 32. Charge Deposition Profile for the Sn/Sn/Al Configuration

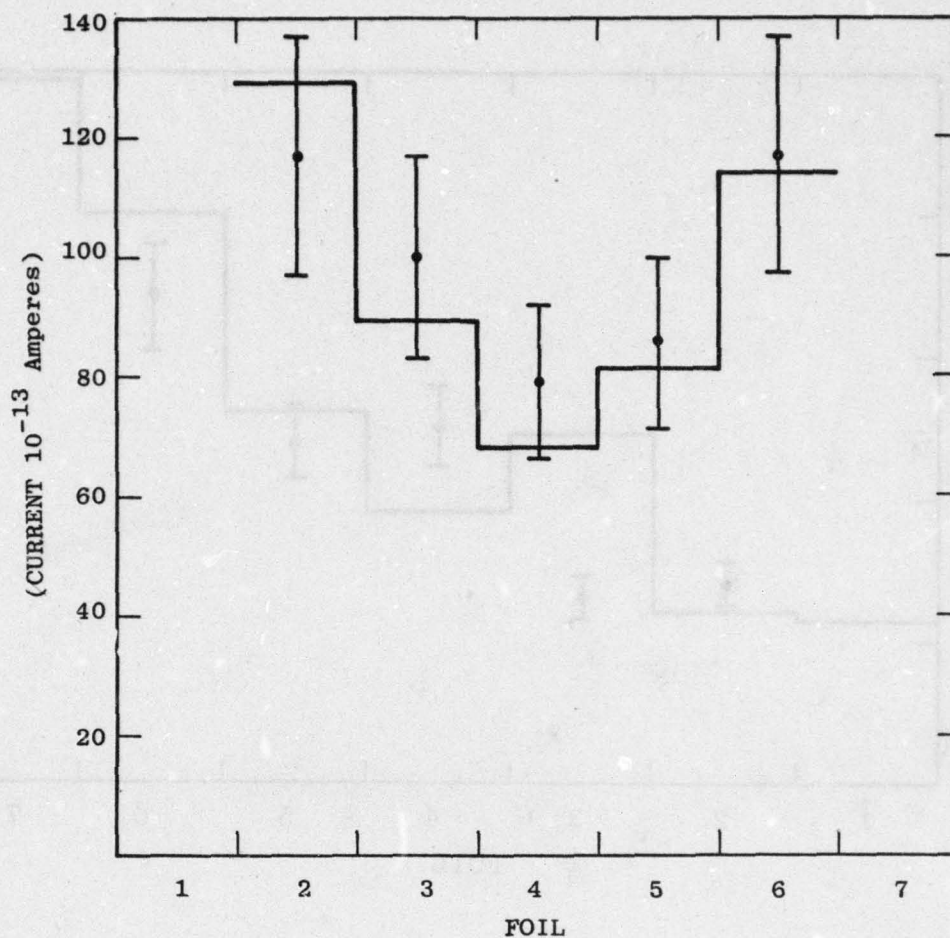


FIGURE 33. Charge Deposition Profile for the Al-Ta-Al Configuration

DISTRIBUTION LIST

DEPARTMENT OF DEFENSE

Defense Communication Engineer Center
1860 Wiehle Ave
Reston, VA 22090
Attn: Code R320 C W Bergman
Attn: Code R410 J W McClean

Director
Defense Communications Agency
Washington, DC 20305
Attn: Code 540.5
Attn: Code 930 M I Burgett Jr

Defense Documentation Center
Cameron Station
Alexandria, VA 22314
Attn: TC

Director
Defense Intelligence Agency
Washington, DC 20301
Attn: DS-4A2

Director
Defense Nuclear Agency
Washington, DC 20305
Attn: TITL Tech Library
Attn: DDST
Attn: RAEV
Attn: STVL

Dir of Defense Resch & Engineering
Department of Defense
Washington, DC 20301
Attn: S&SS (OS)

Commander
Field Command
Defense Nuclear Agency
Kirtland AFB, NM 87115
Attn: FCPR

Director
Interservice Nuclear Weapons School
Kirtland AFB, NM 87115
Attn: Document Control

Director
Joint Strat Tgt Planning Staff JCS
Offutt AFB Omaha, NB 68113
Attn: JLTW-2

Chief
Livermore Division Fld Command DNA
Lawrence Livermore Laboratory
P.O. Box 808
Livermore, CA 94550
Attn: FCPRL

Director
National Security Agency
Ft. George G. Meade, MD 20755
Attn: O O Van Gunten R-425
Attn: TDL

DEPARTMENT OF ARMY

Project Manager
Army Tactical Data Systems
US Army Electronics Command
Fort Monmouth, NJ 07703
Attn: DRCPN-TDS-SD
Attn: DWAIN B Huewe

Commander
BMD System Command
P.O. Box 1500
Huntsville, AL 35807
Attn: BDMSC-TEN

Commander
Frankford Arsenal
Bridge and Tacony Sts
Philadelphia, PA 19137
Attn: SARFA FCD

Commander
Harry Diamond Laboratories
2800 Powder Mill Road
Adelphi, MD 20783
Attn: DRXDO-EM.
Attn: DRXDO-NP
Attn: DRXDO-TI/Tech Library.
Attn: DRXDO-RB
Attn: DRXDO-RCC.
Attn: DRXDO-RC.
Attn: J Halpin.
Attn: J McGarrity.

Commanding Officer
Night Vision Laboratory
US Army Electronics Command
Fort Belvoir, VA 22060
Attn: Capt. Allan S Parker

Commander
Picatinny Arsenal
Dover, NJ 07801
Attn: SMUPA-FR-S-P
Attn: SARPA-FR-E
Attn: SMUPA-ND-W
Attn: SMUPA-ND-D-B
Attn: SARPA-ND-C-E
Attn: SARPA-ND-N
Attn: SMUPA-ND-N-E

Commander
Redstone Scientific Information Center
US Army Missile Command
Redstone Arsenal, AL 35809
Attn: Chief, Documents

Secretary of the Army
Washington, DC 20310
Attn: ODUSA or D Willard

Director
Trasana
White Sands Missile Range NM 88002
Attn: ATAA-EAC

Director
US Army Ballistic Research Labs
Aberdeen Proving Ground, MD 21005
Attn: DRXBR-X
Attn: DRXBR-VL
Attn: DRXBR-AM
Attn: DRXRD-BVL

Chief
US Army Communications Systems Agency
Fort Monmouth, NJ 07703
Attn: SCCM-AD-SV/Library

Commander
US Army Electronics Command
Fort Monmouth, NJ 07703
Attn: DRSEL-TL-IR
Attn: DRSEL-CE
Attn: DRSEL-CT-HDK
Attn: DRSEL-GG-TD
Attn: DRSEL-TL-MD
Attn: DRSEL-TL-ND
Attn: DRSEL-PL-ENV

Commandant
US Army Engineer School
Ft Belvoir VA 22060
Attn: ATSE-CTD-CS

Commander-in-Chief
US Army Europe & Seventh Army
APO New York 09403
(Heidelberg)
Attn: ODCSE-E AEAGE-PI

Commandant
US Army Field Artillery School
Fort Sill, OK 73503
Attn: ATSFA-CTD-ME

Commander
US Army Material Dev & Readiness CMD
5001 Eisenhower Ave
Alexandria, VA 22333
Attn: DRCDE-D

Commander, US Army Missile Command
Redstone Arsenal, AL 35809
Attn: DRSI-RGP
Attn: DRCPM-PE-EA
Attn: DRSMI-RGD
Attn: DRSMI-RGP
Attn: DRSMI-RRR

Chief
US Army Nuc & Chemical Surety GP
Bldg 2073, North Area
Ft Belvoir, VA 22060
Attn: MOSG-ND

Commander
US Army Nuclear Agency
7500 Backlick Road
Building 2073
Springfield, VA 22150
Attn: ATCN-W

Commander
US Army Tank Automotive Command
Warren, MI 48090
Attn: DRCPM-GCM-SW

Commander
White Sands Missile Range
White Sands Missile Range NM 88002
Attn: STEWS-TE-NT

DEPARTMENT OF NAVY

Chief of Naval Research
Navy Department
Arlington, VA 22217
Attn: Code 427

Commander Officer
Naval Avionics Facility
21st & Arlington Ave
Indianapolis, IN 46218
Attn: Branch 942

Commander
Naval Electronic Systems Command Hqs
Washington, DC 20360
Attn: Code 504511
Attn: Code 50451
Attn: PME 117-21
Attn: Code 5032
Attn: Flex 05323

Commanding Officer
Naval Intelligence Support Ctr
4301 Suitland Road, Bldg. 5
Washington, DC 20390
Attn: NISC-45

Director
Naval Research Laboratory
Washington, DC 20375
Attn: Code 4004
Attn: Code 6631
Attn: Code 5210
Attn: Code 5216
Attn: Code 6460
Attn: Code 601
Attn: Code 7701
Attn: Code 2627

Commander
Naval Sea Systems Command
Navy Department
Washington, DC 20362
Attn: SEA-9931

Officer-in-Charge
Naval Surface Weapons Center
White Oak, Silver Spring, MD 20910
Attn: Code WA52
Attn: Code WA501/Navy Nuc Prgms Off
Attn: Code WA50

Commander
Naval Weapons Center
China Lake, CA 9355
Attn: Code 533 Tech Library

Commanding Officer
Naval Weapons Evaluation Facility
Kirtland AFB Albuquerque, NM 87117
Attn: Code ATG/Mr Stanley

Commanding Officer
Naval Weapons Support Center
Crane, IN 47522
Attn: Code 7024/J Ramsey
Attn: Code 70242/J A Munarin

Commanding Officer
Nuclear Weapons TNG Center Pacific
Naval Air Station, North Island
San Diego, CA 92135
Attn: Code 50

Director
Strategic Systems Project Office
Navy Department
Washington, DC 20376
Attn: SP 2701
Attn: NSP-2342
Attn: NSP-27331

DEPARTMENT OF THE AIR FORCE

RADC/Deputy for Electronic Technology
Hanscom AFB, MA 01731
Attn: ET/Stop 30/E Cormier
Attn: ES/Stop 30/F Shepherd
Attn: ES/Stop 30/E A Burke

AF Institute of Technology, AU
Wright-Patterson AFB, OH 45433
Attn: ENP/C J Bridgman

AF Materials Laboratory, AFSC
Wright-Patterson AFB, OH 45433
Attn: LTE

AF Weapons Laboratory, AFSC
Kirtland AFB, NM 87117
Attn: DES
Attn: ELA
Attn: ELP TREE SECTION
Attn: NT/Carl E Baum
Attn: ELS
Attn: NTS

AFTAC
Patrick AFB FL 32925
Attn: TFS/Maj M F Schneider

AF Avionics Laboratory, AFSC
Wright-Patterson AFB, OH 45433
Attn: DHE/H J Hennecke
Attn: DHM/C Friend
Attn: DH/Ltc McKenzie
Attn: AAT/M Friar

Commander
ASD
Wright-Patterson AFB, OH 45433
Attn: ASD/ENESS/P T Marth
Attn: ASD-YH-EX/Ltc R Leverette
Attn: ENACC/R L Fish

Hq ESD
Hanscom AFB, MA 01731
Attn: YSEV

Hq ESD
Hanscom AFB, MA 01731
Attn: YWET

Commander
Foreign Technology Division, AFSC
Wright-Patterson AFB, OH 45433
Attn: FTDP

Commander
Rome Air Development Center, AFSC
Griffiss AFB, NY 13440
Attn: RBRP
Attn: RBRAC

Commander
RADC/Deputy for Electronic Technology
Hanscom AFB, MA 01731
Attn: ES/A Kahan
Attn: ES/B Buchanan
Attn: ES/R Dolan

SAMSO/YE
Post Office Box 92960
Worldway Postal Center
Los Angeles, CA 90009
Attn: YEE

SAMSO/IN
Post Office Box 92960
Worldway Postal Center
Los Angeles, CA 90009
Attn: IND/I J Judy

SAMSO/MN
Norton AFB, CA 92409
Attn: MNNH

SAMSO/RS
Post Office Box 92960
Worldway Postal Center
Los Angeles, CA 90009
Attn: RSMG
Attn: RSSE

SAMSO/SK
Post Office Box 92960
Worldway Postal Center
Los Angeles, CA 90009
Attn: SKF

SAMSO/SZ
Post Office Box 92960
Worldway Postal Center
Los Angeles, CA 90009
Attn: SZJ

Commander in Chief
Strategic Air Command
Offutt AFB, NB 68113
Attn: XPFS
Attn: NRI-STINFO Library

US ENERGY RSCH & DEV ADMIN
University of California
Lawrence Livermore Laboratory
P. O. Box 808
Livermore, CA 94550
Attn: Hans Kruger L-96.
Attn: Frederick R Kovar L-31
Attn: Donald J Meeker L-545
Attn: Tech Info Dept L-3.
Attn: F K Miller L-156
Attn: William J Hogan L-531
Attn: Ronald L Ott L-531.
Attn: Joseph E Keller Jr L-125.
Attn: Lawrence Cleland L-156.

Los Alamos Scientific Laboratory
P. O. Box 1663
Los Alamos NM 87545
Attn: Doc Con for B W Noel
Attn: Doc Con for J A Freed

SANDIA Laboratories
P. O. Box 5800
Albuquerque NM 87115
Attn: Doc Con for Org 2110/J A Hood
Attn: Doc Con for 3141 Sandia Rpt Coll
Attn: Doc Con for Org 2140/R Gregory

US Energy Research & Dev Admin
Albuquerque Operations Office
P. O. Box 5400
Albuquerque, NM 87115
Attn: Doc Con for WSSB

OTHER GOVERNMENT

Department of Commerce
National Bureau of Standards
Washington, DC 20234
Attn: Judson C French

**DEPARTMENT OF DEFENSE
CONTRACTORS**

Aerojet Electro-Systems Co.
Div of Aerojet-General Corp.
P. O. Box 296, 1100 W. Hollyvale Dr
Azusa, CA 91702
Attn: T D Hanscome

Aerospace Corp.
P. O. Box 92957
Los Angeles, CA 90009
Attn: John Ditre
Attn: Irving M Garfunkel
Attn: S P Bower
Attn: Julian Reinheimer
Attn: L W Aukerman
Attn: Library
Attn: William W Willis

Analog Technology Corp.
3410 East Foothill Boulevard
Pasadena, CA 91107
Attn: J J Baum

AVCO Research & Systems Group
201 Lowell St
Wilmington, MA 01887
Attn: Research Lib/A830 Rm 7201

BDM Corp.
7915 Jones Branch Drive
McClean, VA 22101
Attn: T H Neighbors

EDM Corporation
P. O. Box 9274
Albuquerque International
Albuquerque, NM 87119
Attn: D R Alexander

Bendix Corp.
Communication Division
East Joppa Road
Baltimore, MD 21204
Attn: Document Control

Bendix Corp.
Research Laboratories Division
Bendix Center
Southfield, MI 48075
Attn: Mgr Prgm Dev/D J Niehaus
Attn: Max Frank

Boeing Company
P. O. Box 3707
Seattle, WA 98124
Attn: H W Wicklein/MS 17-11
Attn: Itsu Amura/2R-00
Attn: Aerospace Library
Attn: R S Caldwell/2R-00
Attn: Carl Rosenberg/2R-00

Booz-Allen and Hamilton, Inc.
106 Apple Street
Tinton Falls, NJ 07724
Attn: Raymond J Chrisner

California Institute of Technology
Jet Propulsion Laboratory
4800 Oak Grove Drive
Pasadena, CA 91103
Attn: J Bryden
Attn: A G Stanley

Charles Stark Draper Laboratory Inc.
555 Technology Square
Cambridge, MA 02139
Attn: Kenneth Fertig
Attn: Paul R Kelly

Cincinnati Electronics Corp.
2630 Glendale - Milford Road
Cincinnati, OH 45241
Attn: Lois Hammond
Attn: C R Stump

Control Data Corporation
P. O. Box 0
Minneapolis, MN 55440
Attn: Jack Meehan

Cutler-Hammer, Inc.
AIL Division
Comac Road
Deer Park, NY 11729
Attn: Central Tech Files/A Anthony

Dikewood Industries, Inc.
1009 Bradbury Drive, S. E.
Albuquerque, NM 87106
Attn: L Wayne Davis

E-Systems, Inc.
Greenville Division
P. O. Box 1056
Greenville, TX 75401
Attn: Library 8-50100

Effects Technology, Inc.
5383 Hollister Avenue
Santa Barbara, CA 93111
Attn: Edward J Steele

Exp & Math Physics Consultants
P. O. Box 66331
Los Angeles, CA 90066
Attn: Thomas M Jordan

Fairchild Camera & Instrument Corp.
464 Ellis St
Mountain View, CA 94040
Attn: Sec Dept for 2-233 D K Myers

Fairchild Industries, Inc.
Sherman Fairchild Technology Center
20301 Century Boulevard
Germantown, MD 20767
Attn: Mgr Config Data & Standards

Florida, University of
P. O. Box 284
Gainesville, FL 32601
Attn: Patricia B Rambo
Attn: D P Kennedy

Ford Aerospace & Communications Corp.
3939 Fabian Way
Palo Alto, CA 94303
Attn: Edward R Hahn/MS-X22
Attn: Donald R McMorrow/MS-G30
Attn: Samuel R Crawford/MS-531

Ford Aerospace & Comm Operations
Ford & Jamboree Roads
Newport Beach, CA 92663
Attn: F R Poncelet Jr.
Attn: Ken C Attinger
Attn: Tech Info Section

Franklin Institute, The
20th St and Parkway
Philadelphia, PA 19103
Attn: Ramie H Thompson

Garrett Corporation
P. O. Box 92248, 9851 Sepulveda Blvd
Los Angeles, CA 90009
Attn: Robert E Weir/Dept 93-9

General Dynamics Corp.
Electronics Div Orlando Operations
P. O. Box 2566
Orlando, FL 32802
Attn: D W Coleman

General Electric Company
Space Division
Valley Forge Space Center
Goddard Blvd King of Prussia
P. O. Box 8555
Philadelphia, PA 19101
Attn: Larry I Chasen
Attn: John L Andrews
Attn: Joseph C Peden/VFSC, Rm 4230M

General Electric Company
Re-Entry & Environmental Systems Div
P. O. Box 7722
3198 Chestnut St
Philadelphia, PA 19101
Attn: Robert V Benedict
Attn: John W Palchefskey Jr
Attn: Ray E Anderson

General Electric Company
Ordnance Systems
100 Plastics Ave.
Pittsfield, MA 01201

General Electric Company
Tempo-Center for Advanced Studies
816 State St (P O Drawer QQ)
Santa Barbara, CA 93102
Attn: Royden R Rutherford
Attn: DASIAC
Attn: M Espig
Attn: William McNamera

AD-A062 332

SCIENCE APPLICATIONS INC MCLEAN VA
SOFT X-RAY PHOTOEMISSION AND CHARGE DEPOSITION NEAR MATERIAL IN--ETC(U)
AUG 78 D J STRICKLAND, D L LIN, V W PINE F19628-77-C-0181
RADC-TR-78-183 NL

UNCLASSIFIED

2 OF 2

AD
A062332



END
DATE
FILMED

3--79

DDC

General Electric Company
Aircraft Engine Business Group
Evendale Plant Int Hwy 75 S
Cincinnati, OH 45215
Attn: John A Ellerhorst E2

General Electric Company
Aerospace Electronics Systems
French Road
Utica, NY 13503
Attn: Charles M Hewison/Drop 624
Attn: W J Patterson/Drop 233

General Electric Company
P. O. Box 5000
Binghamton, NY 13902
Attn: David W Pepin/Drop 160

General Electric Company-Tempo
c/o Defense Nuclear Agency
Washington, DC 20305
Attn: DASIAC
Attn: William Alfonte

General Research Corporation
P. O. Box 3587
Santa Barbara, CA 93105
Attn: Robert D Hill

Georgia Institute of Technology
Georgia Tech Research Institute
Atlanta, GA 30332
Attn: R Curry

Grumman Aerospace Corporation
South Oyster Bay Road
Bethpage, NY 11714
Attn: Jerry Rogers/Dept 533

GTE Sylvania, Inc.
Electronics Systems GRP-Eastern Div
77 A St
Needham, MA 02194
Attn: Charles A Thornhill, Librarian
Attn: James A Waldon
Attn: Leonard L Blaisdell

GTE Sylvania, Inc.
189 B St
Needham Heights, MA 02194
Attn: Paul B Fredrickson
Attn: Herbert A Ullman
Attn: H & V Group
Attn: Charles H Ramsbottom

Gulton Industries, Inc.
Engineered Magnetics Division
13041 Carise Ave
Hawthorne, CA 90250
Attn: Engnmagnetics Div

Harris Corp.
Harris Semiconductor Division
P. O. Box 883
Melbourne, FL 32901
Attn: Wayne E Abare/MS 16-111
Attn: Carl F Davis/MS 17-220
Attn: T L Clark/MS 4040

Hazeltine Corp.
Pulaski Rd
Greenlawn, NY 11740
Attn: Tech Info Ctr/M Waite

Honeywell Inc.
Avionics Division
2600 Ridgeway Parkway
Minneapolis, MN 55413
Attn: Ronald R Johnson/A1622
Attn: R J Kell/MS S2572

Honeywell Inc.
Avionics Division
13350 US Highway 19 North
St Petersburg, FL 33733
Attn: H H Noble/MS 725-5A
Attn: S H Graaff/MS 725-J

Honeywell Inc.
Radiation Center
2 Forbes Road
Lexington, MA 02173
Attn: Technical Library

Hughes Aircraft Company
Centinela and Teale
Culver City, CA 90230
Attn: Dan Binder/MS 6-D147
Attn: Billy W Campbell/MS 6-E-110
Attn: Kenneth R Walker/MS D157
Attn: John B Singletary/MS 6-D133

Hughes Aircraft Co., El Segundo Site
P. O. Box 92919
Los Angeles, CA 90009
Attn: William W Scott/MS A1080
Attn: Edward C Smith/MS A620

IBM Corporation
Route 17C
Owego, NY 13827
Attn: Frank Frankovsky
Attn: Harry W Mathers/Dept M41

Intl Tel & Telegraph Corp
500 Washington Ave
Nutley, NY 07110
Attn: Alexander T Richardson

Ion Physics Corp.
South Bedford St
Burlington, MA 01803
Attn: Robert D Evans

IRT Corp.
P. O. Box 81087
San Diego, CA 92138
Attn: MDC
Attn: Leo D Cotter
Attn: R L Mertz

JAYCOR
205 S. Whitting St, Suite 500
Alexandria, VA 22304
Attn: Catherine Turesko
Attn: Robert Sullivan

Johns Hopkins University
Applied Physics Laboratory
Johns Hopkins Road
Laurel, MD 20810
Attn: Peter E Partridge

Kaman Sciences Corp.
P. O. Box 7463
Colorado Springs, CO 80933
Attn: Jerry I Lubell
Attn: Walter E Ware
Attn: John R Hoffman
Attn: Donald H Bryce
Attn: Albert P Bridges
Attn: W Foster Rich

Litton Systems, Inc.
Guidance & Control Systems Division
5500 Canoga Ave
Woodland Hills, CA 91364
Attn: John P Retzler
Attn: Val J Ashby/MS 67
Attn: R W Maughmer

Litton Systems, Inc.
Electron Tube Division
1035 Westminster Drive
Williamsport, PA 17701
Attn: Frank J McCarthy

Lockheed Missiles & Space Co. Inc.
P. O. Box 504
Sunnyvale, CA 94088
Attn: B T Kimura/Dept 81-14
Attn: E A Smith/Dept 85-85
Attn: George F Heath/Dept 81-14
Attn: Samuel I Taimuty/Dept 85-85
Attn: L Rossi/Dept 81-64

Lockheed Missiles & Space Co. Inc.
3251 Hanover St
Palo Alto, CA 94304
Attn: Tech Info Ctr D/Coll

M.I.T. Lincoln Laboratory
P. O. Box 73
Lexington, MA 02173
Attn: Leona Loughlin, Librarian A-082

Martin Marietta Aerospace
Orlando Division
P. O. Box 5837
Orlando, FL 32805
Attn: Jack M Ashford/MP-537
Attn: William W Mras/MP-413
Attn: Mona C Griffith/Lib MP-30

Martin Marietta Corp.
Denver Division
P. O. Box 179
Denver, CO 80201
Attn: Paul G Kase/Mail 8203
Attn: Research Lib 6617 J R McKee
Attn: J E Goodwin/Mail 0452
Attn: B T Graham/MS PO-454

McDonnell Douglas Corp.
P. O. Box 516
St Louis, MO 63166
Attn: Tom Ender
Attn: Technical Library

McDonnell Douglas Corp.
5301 Bolsa Ave
Huntington Beach, CA 92647
Attn: Stanley Schneider

McDonnell Douglas Corp.
3855 Lakewood Boulevard
Long Beach, CA 90846
Attn: Technical Library, C1-290/36-84

Mission Research Corp.
735 State St
Santa Barbara, CA 93101
Attn: William C Hart

Mission Research Corp.-San Diego
P. O. Box 1209
La Jolla, CA 92038
Attn: V A J Van Lint
Attn: J P Raymond

The MITRE Corp.
P. O. Box 208
Bedford, MA 01730
Attn: M E Fitzgerald
Attn: Library

National Academy of Sciences
2101 Constitution Ave, NW
Washington, DC 20418
Attn: National Materials Advisory Board
Attn: R S Shane, Nat Materials Advsy

University of New Mexico
Electrical Engineering & Computer
Science Dept
Albuquerque, NM 87131
Attn: Harold Southward

Northrop Corp.
Electronic Division
1 Research Park
Palos Verdes Peninsula, CA 90274
Attn: George H Towner
Attn: Boyce T Ahlport

Northrop Corp.
Northrop Research & Technology Ctr
3401 West Broadway
Hawthorne, CA 90250
Attn: Orlie L Curtis, Jr
Attn: David N Pocock
Attn: J R Srour

Northrop Corp.
Electronic Division
2301 West 120th St
Hawthorne, CA 90250
Attn: Vincent R DeMartino
Attn: Joseph D Russo
Attn: John M Reynolds

Palisades Inst for Resch Services Inc.
201 Varick St
New York, NY 10014
Attn: Records Supervisor

Physics International Co.
2700 Merced St
San Leandro, CA 94577
Attn: Doc Con for C H Stallings
Attn: Doc Con for J H Huntington

R&D Associates
P. O. Box 9695
Marina Del Rey, CA 90291
Attn: S Clay Rogers

Raytheon Company
Hartwell Road
Bedford, MA 01730
Attn: Gajanan H Joshi, Radar Sys Lab

Raytheon Company
528 Boston Post Road
Sudbury, MA 01776
Attn: Harold L Fleischer

RCA Corp.
Government Systems Division
Astro Electronics
P. O. Box 800, Locust Corner
Fast Windsor Township
Princeton, NJ 08540
Attn: George J Brucker

RCA Corporation
Camden Complex
Front & Cooper Sts
Camden, NJ 08012
Attn: E Van Keuren 13-5-2

Rensselaer Polytechnic Institute
P. O. Box 965
Troy, NY 12181
Attn: Ronald J Gutmann

Research Triangle Institute
P. O. Box 12194
Research Triangle Park, NC 27709
Attn: Eng Div Mayrant Simons Jr

Rockwell International Corp.
P. O. Box 3105
Anaheim, CA 92803
Attn: George C Messenger FB61
Attn: Donald J Stevens FA70
Attn: K F Hull
Attn: N J Rudie FA53
Attn: James E Bell, HA10

Rockwell International Corporation
3701 West Imperial Highway
Los Angeles, CA 90009
Attn: T B Yates

Rockwell International Corporation
Collins Divisions
400 Collins Road NE
Cedar Rapids, IA 52406
Attn: Dennis Sutherland
Attn: Alan A Langenfeld
Attn: Mildred A Blair

Sanders Associates, Inc.
95 Canal St
Nashua, NH 03060
Attn: Moe L Aitel NCA 1 3236

Science Applications, Inc.
P. O. Box 2351
La Jolla, CA 92038
Attn: J Robert Beyster

Science Applications, Inc.
Huntsville Division
2109 W Clinton Ave
Suite 700
Huntsville, AL 35805
Attn: Noel R Byrn

Singer Company (Data Systems)
150 Totowa Road
Wayne, NJ 07470
Attn: Tech Info Center

Sperry Flight Systems Division
Sperry Rand Corp.
P. O. Box 21111
Phoenix, AZ 85036
Attn: D Andrew Schow

Sperry Univac
Univac Park, P. O. Box 3535
St. Paul, MN 55165
Attn: James A Inda/MS 41T25

Stanford Research Institute
333 Ravenswood Ave
Menlo Park, CA 94025
Attn: Philip J Dolan
Attn: Archur Lee Whitson

Stanford Research Institute
306 Wynn Drive, NW
Huntsville, AL 35805
Attn: MacPherson Morgan

Sundstrand Corp.
4751 Harrison Ave.
Rockford, IL 61101
Attn: Curtis B White

Systron-Donner Corp.
1070 San Miguel Road
Concord, CA 94518
Attn: Gordon B Dean
Attn: Harold D Morris

Texas Instruments, Inc.
P. O. Box 5474
Dallas, TX 75222
Attn: Donald J Manus/MS 72

Texas Tech University
P. O. Box 5404 North College Station
Lubbock, TX 79417
Attn: Travis L Simpson

TRW Defense & Space Sys Group
One Space Park
Redondo Beach, CA 90278
Attn: Robert M Webb RI 2410
Attn: Tech Info Center/S1930
Attn: O E Adams RI-2036
Attn: R K Plebuch RI-2078

TRW Defense & Space Sys Group
San Bernardino Operations
P. O. Box 1310
San Bernardino, CA 92402
Attn: R Kitter

United Technologies Corp.
Hamilton Standard Division
Bradley International Airport
Windsor Locks, CT 06069
Attn: Raymond G Giguere

Vought Corp.
P. O. Box 5907
Dallas, TX 75222
Attn: Technical Data Ctr

ADDITIONAL DISTRIBUTION LIST

Windsor AFB, MA 01731
Attn: AFGL/SUSRP/Stop 30
Attn: AFGL/CC/Stop 30
Attn: AFGL/SUOL/Stop 20
Attn: ESD/XR/Stop 30
Attn: ESD/XR/Stop 30/D Brick
Attn: DCD/SATIN IV
Attn: MCAE/Lt Col D Sparks
Attn: ES/Stop 30
Attn: EE/Stop 30

Griffiss AFB, NY 13441
Attn: RADC/OC
Attn: RADC/IS
Attn: RADC/DC

Attn: RADC/IR
Attn: RADC/CA
Attn: RADC/TIR
Attn: RADC/DAP
Attn: RADC/TILD

Maxwell AFB, AL 36112
Attn: AUL/LSE-67-342

US Army Missile Command Labs
Redstone Scientific Information Ctr
Redstone Arsenal, AL 35809
Attn: Chief, Documents

SAMSO (YA/AT)
P. O. Box 92960
Worldway Postal Center
Los Angeles, CA 90009
Attn: Mr Hess

Naval Postgraduate School
Superintendent
Monterey, CA 93940
Attn: Library (Code 2124)

US Dept. of Commerce
Boulder Laboratories
Boulder, CO 80302
Attn: Library/NOAA/ER1

USAF Academy
Library
Colorado 80840
Attn: 80840

Eglin AFB, FL 32542
Attn: ADTC/DLOSL

Scott AFB, IL 62225
Attn: AWS/DNTI/Stop 400

NASA Scientific & Technical
Information Facility
P. O. Box 33
College Park, MD 20740

NASA Goddard Space Flight Center
Goddard Space Flight Center
Greenbelt, MD 20771
Attn: Technical Library, Code 252,
Bldg. 21

Naval Surface Weapons Center
White Oak Lab.
Silver Spring, MD 20910
Attn: Library Code 730, RM 1-321

US Naval Missile Center
Point Mugu, CA 93041
Attn: Tech. Library - Code N0322

NASA Johnson Space Center
Attn: JM6, Technical Library
Houston, TX 77058

NASA
Lewis Research Center
21000 Brookpark Road
Cleveland, OH 44135
Attn: Technical Library

Wright-Patterson AFB, OH 45433
Attn: AFAL/CA
Attn: AFIT/LD, Bldg. 640, Area B
Attn: ASD/ASFR
Attn: ASD/FTD/ETID

Defense Communications Engineering
Center
1860 Wiehls Ave
Reston, VA 22090
Attn: Code R103R

Director, Technical Information
DARPA
1400 Wilson Blvd.
Arlington, VA 22209

Department of the Navy
800 North Quincy St
Arlington, VA 22217
Attn: ONRL Documents, Code 102IP

SAMSO
P. O. Box 92960
Worldway Postal Center
Los Angeles, CA 90006
Attn: Lt Col Staubs

US Army Electronics Command
Fort Monmouth, NJ 07703
Attn: AMSEL-GG-TD

Kirtland AFB NM 87117
Attn: AFWL/SUL Technical Library

US Naval Weapons Center
China Lake, CA 93555
Attn: Technical Library

Los Alamos Scientific Lab.
P. O. Box 1663
Los Alamos, NM 87544
Attn: Report Library

Hq DNA
Washington DC 20305
Attn: Technical Library

Secretary of the Air Force
Washington DC 20330
Attn: SAFRD

Scott AFB IL 62225
Attn: ETAC/CB/Stop 825

Andrews AFB
Washington DC 20334
Attn: AFSC/DLC

Army Material Command
Washington, DC 20315
Attn: AMCRD

NASA Langley Research Center
Langley Station
Hampton, VA 23365
Attn: Technical Library/MS 185

NASA
Washington DC 20546
Attn: Library (KSA-10)

Andrews AFB
Washington, DC 20334
Attn: AFSC/DLS

AFOSR, Bldg 410
Bolling AFB, Washington DC 20332
Attn: CC

AFML
Wright Patterson AFB, OH 45433

The Pentagon
Room 3-D-139
Washington, DC 20301
Attn: ODDR&E-OSD (Library)

ONR (Library)
Washington, DC 20360

Defense Intelligence Agency
Washington, DC 20301
Attn: SO-3A

AFAL
Wright-Patterson AFB, OH 45433
Attn: WRA-1/Library
Attn: TSR-5/Technical Library

Advisory Group on Electron Devices
201 Varick St, 9th Floor
New York, NY 10014

White Sands Missile Range, NM 88002
Attn: STEWS-AD-L/Technical Library

University of New Mexico
Dept of Campus Security & Police
1821 Roma, NE
Albuquerque, NM 87106
Attn: D Neaman

Health and Safety Division
Oak Ridge National Laboratory
P.O. Box X
Oak Ridge Tenn. 37830
Attn: Dr. J. Ashley

AFWL/DYC/Frank P. Cassisa
Kirtland AFB Albuquerque NM 87117

RADC/ESR/Stop 30/C. A. McCartney
Hanscom AFB MA 01731

